SPACE-BORNE HYDROGEN MASER DESIGN

R. F. C. Vessot, M. W. Levine, E. M. Mattison, T. E. Hoffman,
E. A. Imbier, M. Tetu,* and G. Nystrom
(Smithsonian Astrophysical Observatory),
J. J. Kelt, Jr., H. F. Trucks, and J. L. Vaniman
(Marshall Space Flight Center)

ABSTRACT

The gravitational redshift rocket probe experiment, with a specially developed space-qualified hydrogen maser as the principal component of the payload, was successfully flown July 18, 1976. The experiment strategy and the requirements for the maser are reviewed, and the design features developed to meet the requirements are described. Stability data of the space maser taken during the flight with a three-link doppler canceling system are discussed.

INTRODUCTION

The objective of the gravitational-redshift experiment is to compare the rate of a space-borne clock (representing the "proper" clock of idealized relativity "gedanken" experiments) moving over a wide range of gravitational potential against a set of clocks in a constant gravitational potential. This experiment was realized June 18, 1976, by using a clock launched into space in a nearly vertical trajectory whose apogee altitude was about 10000 km. This paper will concentrate on the design aspect of the space maser used in that experiment.

The gravitational-redshift rocket-probe experiment was performed jointly by the Smithsonian Astrophysical Observatory (SAO) and the

*Currently at Laval University, Quebec City, Canada.

George C. Marshall Space Flight Center of the National Aeronautics Space Administration (NASA/MSFC). At the present time, although the final data have yet to be generated, the experiment has successfully met its objectives. The following is an account of some aspects of the design of the maser for space and the rationale behind some technical decisions made to meet a very stringent set of environmental and weight restrictions. In addition, this paper serves to update an early description of the maser published in 1974[1]; in the hardware description of that report, the fourth-stage rocket motor was still to remain attached to the spin-stabilized payload.

The gravitational-redshift rocket-probe experiment evolved from the originally proposed 24-hour eccentric-orbit experiment powered by a Titan 3C system[2-4] in order to make use of the far more modest Scout D propulsion system. The experiment became a one-shot up-down comparison of a probe oscillator with a ground oscillator, and the strategy for the experiment became considerably more demanding than originally planned for the orbital mission.

From the dynamics of a body falling nearly vertically in the gravity field of the earth and from the known behavior of atomic hydrogen masers, we can establish a very rough optimum situation, based on the following considerations:

A. Allow enough time aloft to stabilize whatever launch-induced perturbations may occur and minimize the effect of such thermal and mechanical perturbations so that the maximum possible stable operating time is available.

B. Keep the payload in communication with the ground station throughout the mission, concentrating on obtaining data from apogee down to altitudes as low as possible at the end of the mission.

Owing to the 1/R gravity potential acting on a freely falling body, the time available for measurements near impact is a relatively insensi-

tive function of the time aloft, and the strategy therefore is to obtain a minimum period of about 2 hours, attaining apogee redshift values greater than 4 parts in 10^{10}. The upward branch of the trajectory would also contain some data; however, because of the propulsion phase and payload stabilizing time, these data will be of less value than the data from the later, downward branch.

Obviously, no time would be available for the more conventional spacecraft outgassing and thermal stabilizing. Furthermore, since it would be a one-shot mission, both the space and the ground equipment would have to operate without interruption and with the required stability throughout the mission. The experiment had to start from a very stable operating condition before launch and maintain thermal and mechanical stability throughout. This plus the weight limitations resulting from the vehicle constraints placed rather stringent design requirements on the experiment.

The hypothesis being tested is that the rate of the proper clock will vary according to the expression

$$\frac{\Delta f}{f} = \alpha \frac{\Delta \phi}{c^2} \quad ,$$

where $\Delta f/f$ is the fractional shift observed in the proper clock, $\Delta\phi$ is the variation in the gravitational potential of the clock, and c is the velocity of light. The parameter α is taken as unity according to the principle of equivalence, and departures from unity in this test will be given by ε, where $\alpha = 1 \pm \varepsilon$. The best previous test, made over a 75-ft vertical distance by using the Fe_{57} Mossbauer effect, was done in the early 1960s by R. V. Pound, G. A. Rebka, and J. L. Snider, who placed a 1% limit on ε.

Our goal is to test the above expression for $\Delta\phi/c^2$ to as high a precision as possible. Ignoring all other perturbations in the system, the maximum objective is limited by the relative stability of the maser clocks, which, for 100-sec averaging intervals and beyond, is assumed to be 1 part in 10^{14}. Therefore, for $\Delta\phi/c^2 \sim 4 \times 10^{-10}$, the precision of the test is constrained to a 25-ppm upper limit. The system for removing the first-order and ionospheric doppler effects is shown in Figure 1.

The design strategy for the experiment is to make all other contributions of system instability well below 1 part in 10^{14} for time intervals from 100 sec to the end of the flight.

MASER DESIGN REQUIREMENTS

The first requirement is that of survival through the vibration, shock, acoustical pressures, and decompression of launch by the four-stage, solid-fueled Scout system into a zero g and spinning condition while in space. Of the total payload equipment, the hydrogen maser and the newly designed ammonia cooling system for the transponder are the only types of items that had not previously been flown in space.

At the outset, we allowed about 90 lb for the maser and adhered as closely as possible to this limit. The requirements for its survival and operation in space were as follows:

A. The maser-frequency fixed-frequency offset resulting from the trauma of launch should be small, less than 5 parts in 10^{12}, stabilizing within about 10 min to an overall stability of 1 part in 10^{14} for the remainder of the mission.

B. Thermal, zero g, spin, and pressure effects from the transition into space causing possible longer term instability must be less than 1×10^{-14} either by calibrating for various environmental factors during

preflight simulation tests or by engineering the maser to cope with its immediate environment at this level of stability.

C. The maser should be built so as to operate continuously for about 9 months to allow time for its qualification testing and calibration and to permit it to operate, without alteration, as a piece of flight hardware; this includes several weeks of preflight stabilization.

MASER FREQUENCY PERTURBATIONS

The principal systematic frequency variation of hydrogen masers is described by the following expression:

$$\frac{\Delta f}{f} = \frac{1}{f}\left[\frac{Q_c}{Q_\ell}(f_c - f_0) + 2750\ B^2\right] \quad . \tag{1}$$

The first term is the cavity-resonance mistuning, or "pulling," effect, and the second is the second-order magnetic-field dependence of the atomic hydrogen hyperfine transition $F = 1,\ M_F = 0 \rightarrow F = 0,\ M_F = 0$. Q_c is the cavity resonator Q, and Q_ℓ is the Q of the atomic transition, which depends on the geometry of the hydrogen-maser storage bulb, the quality of the wall coating, and the collision rate of the atoms among themselves (spin-exchange processes). This last process is a function of beam input flux, which, in turn, can be represented in terms of the maser output power level.

Two aspects of the cavity-resonance shift especially concern us: 1) the variation in Δf_c during the mission, and 2) the average magnitude of Δf_c as a result of the combination of shake, shock, and zero gravity that occurs from earth-bound conditions through to the free-fall condition after powered flight ceases. The effect of cavity-resonance variations is obvious in equation (1). However, if there is also a large fixed offset $(f_c - f_0)$, we are further subject to output frequency

variations due to variations in Q_ℓ resulting from changes in atomic hydrogen flux during the mission. These changes in flux result in changes in power level W, and the measured power level was used as a measure of the beam flux for calibration.

In the probe maser, the cavity-resonance frequency is subject to many changes — in the gas pressure P of the enclosure surrounding the cavity vacuum system, in temperature T, in rotation rate Ω (centrifugal stretching), and in the magnetic field B of the microwave ferrite isolator in the output radio-frequency line from the maser cavity. This last effect, found during magnetic calibration of the probe maser, was traced to the isolator ferrite's magnetic resonance; it turns out that this resonance is affected by external fields despite what had previously seemed to be adequate levels of magnetic shielding about the isolator.

The expression describing all the known perturbations to the output frequency of the maser is

$$\frac{df}{f} = \frac{1}{f}\left[\frac{Q_c}{Q_\ell}\left(\frac{\partial f_c}{\partial P}\,dP + \frac{\partial f_c}{\partial T}\,dT + \frac{\partial f_c}{\partial \Omega}\,d\Omega + \frac{\partial f_c}{\partial B}\,dB\right)\right] + Q_c \Delta f_c \frac{\partial (1/Q)}{\partial W}\,dW + \frac{\partial f}{\partial B_0}\,dB_0$$

In the magnetic calibration of the maser, we found that the cavity effect dominated, and the calibration correction includes both effects simultaneously.

The magnetic-field behavior was measured by simulating the magnetic history of the payload before launch, during launch, and throughout the flight. A standard initial-condition state magnetization of the magnetic shields was ensured by a pregaussing operation performed before the vehicle-erection phase of both the actual flight and the magnetic simulation of the flight. We had previously obtained the magnetic

conditions from a survey of the launch area and from measurements at the position of the maser in the launcher while the launcher was being erected. The fields during liftoff and into the trajectory were obtained from earth field models, and the effect of the spinup of the probe at the appropriate earth field is incorporated in the simulation. The simulation of the rapid ascent into the vacuum of space was also included at the appropriate time in the sequence.

The magnetic field encountered during the flight has been determined from standard earth models. At present, only the axial component appears to be important. The algorithm developed for the magnetic influence on the probe output frequency has two branches, owing to hysteresis effects in the magnetic shields. The following algorithm was developed in the magnetic calibrations:

$$\frac{\Delta f}{f} = -5.899 \times 10^{-13} B_{axial} \text{ ascending} \quad ,$$

$$\frac{\Delta f}{f} = -12.721 \times 10^{-13} B_{axial} \text{ descending} \quad .$$

The sign convention is that the plus direction of field enters the earth at its north magnetic pole.

The effect of temperature variations was measured via telemetry in terms of the aft-oven heater voltage. The frequency variation due to this effect was determined during tests, with the following algorithm for frequency versus aft-oven voltage:

$$\frac{\Delta f}{f} = -3.6 \times 10^{-14} \Delta V \quad .$$

The effect of pressure variations measured in the dome enclosing the forward assembly of the maser was determined by calibration to be as follows:

$$\frac{\Delta f}{f} = -2.9 \times 10^{-12} \Delta P \quad ,$$

where ΔP is in psi. The pressure was measured by telemetry.

The effect of spin-rate variations on the output frequency of the maser was measured during tests, from which we developed the following algorithm:

$$\frac{\Delta f}{f} = -4.547 \times 10^{-17} \Omega^{2.05} \quad ,$$

where Ω is in rpm. The spin sensor provided rotation-rate data through the telemetry system.

The effect of the power-level variation is

$$\left.\frac{\Delta f}{f}\right|_{V,\Omega,P} = 1.22 \times 10^{-7} \Delta f_c \Delta W \quad ,$$

where ΔW is in ergs/sec and f_c is in Hz. In these calculations, values of $Q_c = 3.4 \times 10^4$ and $Q_\ell = 1.11 \times 10^9$ were determined for the probe for conditions of flight operation.

During prelaunch testing at MSFC, we established the offset frequency between the probe maser and the ground masers under the conditions at which the probe would be operated. This fixed offset was chiefly due to wall-shift variations in the bulb coatings and to the differences in bulb temperatures, which caused differences in second-order doppler shifts from the stored hydrogen atoms. The importance of this calibration lies in our being able to measure the cavity shift Δf_c when the probe was at apogee, where the time variation of the output beat frequency from the doppler canceling system was least. This estimate of Δf_c enabled us to set the value for the frequency shift due to flux

changes as observed from power changes given by $\left.\frac{\Delta f}{f}\right|_{V,\Omega,P}$ above. The frequency offset at apogee due to relativity must be assumed to be as predicted by the equivalence principle at slightly better than the 1% level for this determination. Our first cut at determining the cavity offset revealed that the cavity was mistuned in frequency by about -36 Hz, which makes

$$\left.\frac{\Delta f}{f}\right|_{V,\Omega,P} = -4.4 \times 10^{-6} \Delta W \quad .$$

MECHANICAL DESIGN

The Cavity-Bulb Structure

The mechanical and thermal requirements of the cavity itself were met by making it of CER-VIT.* Details of the design will follow in later sections; for the present, we must recognize that the overall thermal coefficient of the resonance frequency of the cavity-bulb assembly is about -800 Hz/°C.

At the outset, we realized that the thermal design of the maser would impose a special set of problems, and we established very demanding requirements for temperature excursions at the critical areas near the cavity assembly. Estimates of the temperature variation on the mounting points and the conditions of radiative coupling into space provided the boundary conditions for computer solution at MSFC to help provide design information to SAO for thermal control of the maser.

The maser bulb is a 7"-diameter quartz sphere attached to a cylindrical mounting skirt, also of quartz, by four 1" welds. The

* Owens-Illinois.

skirt, in turn, is fastened to the CER-VIT end plate by means of torr-seal epoxy. The bulb collimator is integral to the bulb structure.

The bulb is coated with FEP-120 Teflon.* The cavity cylinder, made of CER-VIT 101, is 11" in diameter and 9 1/2" long and has an 0.2" wall. The cavity end plates are press moulded of CER-VIT and have reinforcing ribs on the outer surfaces for lightness and stiffness. All interior conducting surfaces of the cavity are coated with evaporated copper about 0.0003" thick. This thin coating is ductile and prevents the cavity from being distorted by thermal expansion of the copper.

The cavity is cut to the appropriate length and the joints lapped for mechanical stability. Before the bulb end plate was released for final assembly, it was shock and vibration tested under vacuum to verify the integrity of all joints – particularly those between the quartz cylinder and the sphere. The cavity is assembled within the vacuum enclosure, as shown in Figure 2, by using a special press that forces the upper end of the vacuum tank to close against the Bellville spring. The previously calibrated behavior of force vs. deflection in the spring was verified during assembly by observing the cavity resonance as the spring was compressed. The CER-VIT cavity in this case acted as a load cell to monitor the applied force. When appropriate load and deflection were achieved, the vacuum tank was welded shut and the tank was removed from the press.

The lower part of the cavity is supported by 12 beryllium copper (BeCu) tangentially oriented rollers seated on a hardened BeCu ring to allow for differential thermal expansion of the aluminum tank cover and the CER-VIT. In the upper assembly, this function is done by the Bellville spring. The vacuum tank has an access port for cavity fine tuning by means of a mechanical adjustment. Electronic fine tuning is done via a loop and varactor diode located in the lower cavity end plate. Dia-

* ®DuPont.

metrically opposite this is the output coupling loop. The cavity components are shown in Figure 3.

The thermal-control system for the probe maser is shown in Figure 4 and discussed in detail in a later section.

Magnetic shielding for the probe maser is interleaved between and supported by layers of machined polyurethane foam insulation, as shown in Figure 5. There are four layers of 0.014" molypermalloy magnetic shields, which, strangely enough, offer better shielding than we can get from 0.032" molypermalloy. The 0.014" thickness is very difficult to handle, very unstable, and easily dented and deformed, all of which can severely deteriorate the shielding factor. The effect of stress is illustrated in Figure 6, which describes the change in shielding factor resulting from stress in the exterior shield.

Figure 7 shows the preamplifiers and voltage-reference electronic boards mounted on the aft-oven cover.

Finally, to complete the description of the cavity-bulb assembly, Figure 8 shows the lightweight C-field solenoid, located inside and close to the innermost magnetic shield. It is wound in three sections; each section is in two layers wound with the same pitch and having the plus and minus leads carefully superimposed to minimize stray magnetic fields from nonsolenoidal current distributions.

The Midplane-Plate Assembly

The main structural member of the experiment — and the structural interface with the spacecraft -- is the aluminum midplane plate, shown in Figure 9. The midplane-plate assembly, 18" in diameter and 1.91" deep, weighs 3.1 lb. The electronics are located in 12 triangular bays, 11 of which house the major portion of the electronics; each bay contains two

printed-circuit cards. The temperature-sensitive electronics are placed on the oven cover just forward of the midplane plate, within the temperature-controlled zones previously described. The remaining bay, which has a test connector at its outermost radius, serves to pass interconnections between the forward and the aft assemblies. The bays are then covered with an 0.062"-thick aluminum plate on which the ancillary equipment aft of the midplane plate is mounted. The aluminum plate provides a precision outside diameter to engage a bore in the spacecraft's mounting plate so that, when the two plates are mated, radial definition is established in two planes. The midplane plate also has 12 mounting holes for securing the experiment in the thrust axis. Figure 9 shows the plate with its wire harness.

The Vacuum Manifold

The aft vacuum assembly (see Figure 10) is a two-pump system: an SAES Getters (Italy) Sorbac cartridge shown in Figure 11 and a Varian 0.2-liter ion pump. The former pump, which works by chemically entrapping hydrogen atoms to form hydrides of zirconium, is the prime hydrogen pump. If the cartridge should become saturated, i.e., unable to pump hydrogen, it can be regenerated by high-temperature bakeout by applying an external voltage to its internal resistance heater and by connecting the maser to a laboratory pumping system to remove the released hydrogen.

The 0.2-liter ion pump is used for noble-gas pumping. Its capacity is sufficient to maintain a system pressure of less than 1×10^{-6} torr for the 9 months before launch. The ion pump also serves as a pressure gauge for the evacuated envelope since the ion current can be correlated with gas pressure.

The aft vacuum assembly also contains a hexapole magnet, mounting ports for the Pirani gauges, and ionization glassware and hydrogen-introduction apparatus.

The hexapole magnet, which was developed by Frequency and Time Systems, Inc., Danvers, Massachusetts, weighs about 2 lb and has a bore of 0.125", a length of 3", and a pole-tip field strength of about 8 kgauss. An 0.050"-diameter glass stopping disk mounted on a tungsten wire at the exit plane of the magnet serves to remove unwanted particles from the beam entering the bulb, such as 1) atoms in the lower magnetic hyperfine levels that are not sufficiently deflected, 2) hydrogen molecules, 3) gases other than hydrogen, and 4) ultraviolet light from the dissociator, which has a strong 1216 Å component that shines directly along the beam through the pores of the collimator and strikes the Teflon coating at the apex of the bulb. Such relatively high-energy ultraviolet light has a very destructive effect on Teflon and in time can break down the long-chain carbon fluorine copolymer.

The dissociation of molecular hydrogen to atomic hydrogen is done in a Pyrex* 7740 glass bulb, 3.5 cm in diameter and 4.5 cm long. Excitation is by a three-turn coil, which is the tank coil for a single-transistor self-oscillator operating at 97 MHz with about 5-watt DC power input. Since we had been having a number of problems with earlier dissociator designs of smaller dimensions, we followed the dimensions successfully used by the maser group at the Jet Propulsion Laboratory.[5] This design has proved to be completely successful and was subsequently used to retrofit all the VLG-10 and 10A ground masers.[6]

To maintain the atomic hydrogen flux level within close limits, we took precautions to keep the temperature very constant by using a forced-air convection circuit. Optical monitoring of the intensity of the dissociator plasma discharge was done with a photodiode and interference-filter combination to measure the strength of the Balmer-α (6562 Å) red line and the light from a spectrally adjacent molecular-hydrogen-band structure. The efficiency of dissociation and the inten-

* ®Corning.

sity of the RF were monitored in this manner. The brightness of the two spectral components, the voltage and current in the dissociator oscillator, the hydrogen pressure, and the maser-signal output were all part of the telemetry information returned to earth during the mission for comparison with data taken during 9 months of continuous and varied tests that were part of the qualification testing program.

Figure 12 describes the assembly of the dissociator, the hydrogen supply, and the pressure control. One of the problems of confining a quantity of hydrogen is the weight of the usual gas bottles. We found that we could use about 1 mol of lithium aluminum hydride ($LiAlH_4$) to supply up to 2 mol of H_2 with a net weight of 38 g. Since thermal dissociation of molecular hydrogen from $LiAlH_4$ is very easily done, we were able to get about 1 mol of H_2 at about 80 psi from approximately 29 g of $LiAlH_4$, controlling the hydrogen flow (and also filtering out impurities and $LiAlH_4$ dust) with a palladium silver diaphragm. Figure 12 shows the pressure-control system used in the probe with the combined thermistor Pirani gauge and vacuum reference gauge, the locations of which can be seen in Figure 10 under the two parallel tubes pointing upward from the aft vacuum bulkhead. Figure 10 also shows the $LiAlH_4$ container in the right-hand foreground. The canister with large holes in it in the left foreground of the photograph is the supporting structure that surrounds and secures the $LiAlH_4$ container.

The assembled payload with its shroud removed is shown in Figure 13. All the components are mounted on a honeycomb plate. The inverted U-shaped structure in the foreground is the radiator that controls the dissociator forced-air temperature-stabilizing system.

PAYLOAD-MASER ELECTRONICS SYSTEMS

The payload electronics systems can be divided, for convenience of description, into seven functional groupings, as follows:

A. Active thermal control and measurement.

B. Atomic hydrogen source control and measurement.

C. Cavity tuning and magnetic-field control.

D. Ion-pump power supply and measurement.

E. Telemetry signal conditioning.

F. Telemetry PCM processor.

G. Auxiliary measurement functions (pressure, spin).

Each of these groupings varies in complexity, in subfunctions required, and in the extent to which support is provided for on-board systems other than the maser itself. Command capability for operating the maser is done by an umbilical cable up to the moment of launch. No in-flight command capability is provided.

Thermal Control

The thermal-control requirements for the maser resonator are extremely stringent. After thermal stabilization on the launch pad, the vacuum-tank temperature at each of three points on the surface of the tank cannot vary by more than 0.01°C throughout the flight. Figure 14 shows a block diagram of the payload-maser electronics assembly.

The thermal-control system serves an additional function: to help maintain the pressure within the outer pressure enclosure constant to within $\pm$0.01 psi. The pressure of the fixed volume of air within the pressure enclosure responds predictably to the temperature of the surface. Therefore, the surface temperature must be closely controlled to minimize pressure changes on the vacuum tank from the trapped air.

A multizone, multilevel, thermal-control system is employed to satisfy the temperature-variation and gradient requirements of the maser. The innermost level of control is the vacuum tank, which immediately

surrounds the maser cavity. The vacuum tank, in turn, is divided into three zones: the forward dome, the tank cylinder, and the aft dome. Each zone is independently controlled with separate thermistor sensors, heater windings, bridge preamplifiers, and power amplifiers. Sensor location, bridge set points, and thermal gains are adjusted to minimize both thermal gradients and changes in thermal gradients with variations in ambient conditions.

The vacuum tank is thermally guarded by the next level of control, the oven. The oven is divided into two zones, the aft-oven cover and the oven forward dome/oven cylinder. Again, each of the zones is independently controlled with sensors located so as to reduce the effects of the ambient temperature on the gradients across the oven. Thermal gains and insulation values are selected so that the oven absorbs the bulk of the ambient-temperature fluctuations, providing a relatively stable environment for the more critical vacuum-tank controllers.

Surrounding the oven is the pressure-can heater. Although this level of control provides some additional thermal isolation for the vacuum tank, its primary function is to maintain the enclosed air in the pressure can at a constant temperature, and therefore at a constant pressure. The pressure can is a single zone, with the sensor location selected to minimize gradients along the can.

All six thermal controllers are virtually identical in electrical design, except for variations in bridge set points and amplifier gains to accommodate different requirements. Figure 15 is a block-diagram representation of a typical controller.

Temperature is sensed by a selected "oceanographic" thermistor, which forms one leg of a bridge; the other three legs are very low-temperature coefficient (±5 ppm/°C) wire-wound resistors. Unbalance of the bridge is detected and amplified by a type 725A integrated-circuit amplifier — an exceptionally stable and low-noise device — and the

output of the 725A is fed back to the bridge. The feedback is positive when the bridge is far off balance, producing an "infinite-gain" or self-oscillating controller. Close to balance, the preamplifier is a true proportional controller with anticipatory feedback.

All the preamplifiers, with the exception of the pressure-can unit, are mounted on the aft-oven cover shown in Figure 7. This volume is controlled to within ± 1°C, contributing further to the overall stability of the controllers and minimizing spurious thermoelectric and thermocouple voltage variations on the thermistor leads.

Each of the preamplifiers feeds a pulse-width-modulated power amplifier with a maximum power capability of 11 watts at minimum battery voltage. The pulse-width-modulated amplifiers operate at a constant pulse rate of approximately 40 kHz; the width of the pulses is proportional to the amplifier input voltage. Thus, the average output voltage is directly proportional to the input voltage, although the power transistors are always operating in a pulse mode, fully on or off. The output of the amplifier is carefully filtered at the output of the final power stage so that only the DC component appears across the output terminals.

The switching amplifier is quite compact and efficient. Overall efficiency is greater than 80% at full load, independent of voltage over the allowable variation in battery voltage. The high efficiency eliminates the requirement for a massive heat sink for the power transistor and permits it to be mounted directly to the amplifier's printed-circuit board. This arrangement simplifies the interconnection wiring and permits the construction of a simple, readily shielded amplifier assembly.

The six thermal-control power amplifiers are mounted on pie-shaped boards, which plug into compartments in the electronics ring as shown in

Figure 16. A simple U-shaped bracket secures the amplifier board and provides a thermal conduction path to the frame of the payload.

The pressure-can preamplifier, which has a much lower stability requirement than the oven or vacuum-tank controllers, is mounted on the aft vacuum assembly.

Thermal Controller Performance

The temperature sensitivity of the thermal-control preamplifiers has been bench tested over a 0° to 60°C range. The maximum allowable variation in bridge-balance temperature is 0.001°C per degree of ambient-temperature change. Typical values are in the order of 0.0001°C/°C, ensuring that the temperature sensitivity of the preamplifiers in the ±1°C aft-oven-cover area does not contribute significantly to the overall temperature sensitivity of the payload maser.

Under more realistic conditions in the thermal-vacuum tests, the thermal-control system maintains the vacuum tank within ±0.01°C under all test conditions.

RF Oscillator Control

The variable-voltage supply for the oscillator collector is furnished by a pulse-width-modulated power amplifier functionally and physically identical to those used in the thermal-control system. The control voltage for the power amplifier is generated by the coarse-control circuitry, also located on a printed-circuit board in the electronics ring. The source control is essentially a 4-bit digital-to-analog converter in which the four digital switches are magnetically latched relays. The relays are set and reset only from the external ground-station equipment. Subsequent payload power interruptions or transients cannot affect the state of the relays.

Hydrogen Pressure Servo

The pressure of the molecular hydrogen gas is in the range of about 1 to 2 millitorr and regulated by a closed-loop servo system. The pressure of the gas is sensed by a Pirani gauge at a point just before the gas line enters the dissociator bulb. The Pirani gauge is a small thermistor bead suspended in the gas volume on two very slender, 0.001", wires. The thermistor forms one leg of a self-balancing bridge. The bridge circuitry causes sufficient current to flow through the bead to make the bead temperature rise to approximately 200°C; at this temperature, the resistance of the bead is such that the bridge is balanced. At very low pressure, little current is required to balance the bridge; at higher pressures, the thermal conductivity of the gas is increased and higher current is required to balance the bridge. Thus, the current required to balance the thermistor bridge is, for a given species of gas, a direct measure of the gas pressure. In order to minimize the effects of ambient-temperature variations of the gas-pressure measurement, a second self-balancing reference bridge is provided. This reference Pirani gauge, which is specially matched to the measurement Pirani, is installed in the high-vacuum side of the vacuum system and exposed to the same ambient temperature as the measurement Pirani. Fluctuations in bridge current are electronically subtracted from the measurement bridge current to provide a temperature-compensated pressure-measurement output.

The pressure-measurement output serves two functions; first, the output level is conditioned and used for telemetry monitoring of hydrogen pressure, and second, it forms one input to the pressure comparator. The other input to the pressure comparator is the pressure-set-point voltage, which is controlled from the GSEE. The pressure comparator provides a voltage output proportional to the difference between the measured pressure and the pressure set point. This voltage output, in turn, serves as the input to the pressure power amplifier.

The power amplifier, identical to the thermal-control power amplifiers, regulates the power input to the $LiAlH_4$ heater and thus completes the feedback loop. The voltage across the canister heater is monitored through the telemetry-signal conditioning system and provides a continuous telemetry record of canister heater power.

The pressure-set-point voltage is generated by a 5-bit digital-to-analog converter. The digital switches are magnetically latched relays that can be operated only from the GSEE system. The two self-balancing bridges, the pressure comparator, and the 5-bit digital-to-analog converter are mounted on the pressure-control assembly, which, in turn, plugs into the electronics ring.

Optical Monitor

The hydrogen-gas discharge in the dissociator bulb must be monitored to obtain information as to the state of dissociation in progress. Two photodetectors are a substitute for direct observation and provide a quantitative, objective measurement of the quality and brightness of the discharge. Each photodetector is an integrated photodiode-amplifier device.

Both the "atomic" and the "molecular" outputs of the optical monitor are signal conditioned and processed for telemetry transmission.

Cavity Tuning and Magnetic-Field Control

The maser cavity is tuned by varying the reverse voltage on a varactor diode mounted within the cavity. The uniform magnetic field imposed on the cavity and storage-bulb area is adjusted by varying the current through a main field winding and two trim windings on the printed-circuit solenoid. These four controllers, one tuning and three magnetic field, are all physically identical and all are installed in the electronics ring.

The cavity-tuning subsystem is shown in block-diagram form in Figure 17. One side of the tuning diode must be frame grounded for RF shielding; therefore, the controller and its associated power supplies must be isolated from frame ground and all other power-supply returns in order to avoid ground loop problems.

The cavity-tuner power supply consists of a DC-to-DC converter that generates +15 and -15 volts, both isolated from ground, from the main battery supply at 24 ± 3 volts. The tuner power supply is mounted on the aft vacuum assembly and is carefully filtered at both the input and the output to avoid injecting noise into the critical cavity-tuning circuitry. This power supply furnishes the operating voltages for the cavity-tuner voltage reference. The reference is essentially an extremely stable voltage regulator generating +10 volts, isolated from ground. The tuner voltage-reference board is located in the temperature-controlled aft-oven-cover area. The +10-volt output of the reference is the input to the cavity-tuner controller, which is a binary 10-bit digital-to-analog converter whose ladder network is a precision thin-film device with a resistance-temperature-tracking coefficient of less than 5 ppm/°C. The digital switches are magnetically latching relays controlled from the payload GSEE. No in-flight command capability is provided.

The 10-bit controller provides an output of 0 to 10 volts to the cavity-tuning varactor with a resolution of approximately 10.0 mvolts per bit. Absolute accuracy is not important, but excellent temperature stability of the varactor voltage is a strong requirement. The temperature coefficient of the voltage reference is 10 ppm/°C; the sensitivity to power-supply variations is essentially zero. The temperature coefficient of the voltage-division ratio of the tuner controller is less than 5 ppm/°C over the temperature range 0° to 70°C.

The current through each of the three windings on the printed-circuit solenoid is adjusted by means of three separate 10-bit binary

digital-to-analog converters, each physically identical to the cavity-tuning controller described above.

Since each winding has a very low resistance, less than 10 ohms, the 0- to 10-volt range of the voltage divider is converted to 0- to 1-mA current by the addition of a 10-kilohm thin-film resistor. An additional relay, not used for the cavity-tuning function, reverses the direction of current flow through the solenoid winding. All 11 magnetically latching relays are controlled directly from the payload GSEE. As before, no switching capability is available after the umbilical cable is removed from the spacecraft.

The 10-bit controller provides an output of 0 to 1 mA through the winding with a resolution of approximately 10 μA per bit. Stability of the current is determined principally by the temperature coefficient of resistance of the series resistor, approximately 50 ppm/°C, over the range 0° to 60°C.

Ion-Pump Power Supply and Measurements

The appendage ion pump requires a power source furnishing approximately 2500 volts at 50 μA maximum. A small DC-to-DC converter, manufactured by MIL Electronics, Lowell, Massachusetts, is mounted directly to the pump bracket. The power-supply high-voltage terminal is adjacent to the pump feedthrough, and the entire high-voltage cavity is potted with a silicone rubber compound after wiring.

The power supply is regulated at 2500 volts $\pm 1\%$ over an input voltage range of 24 ± 3 volts. Current is electronically limited to 50 μamp by internal protective circuitry.

The ion-pump current, which is also a means for measuring the condition of the vacuum, is monitored by measuring the voltage across a

resistor in series with the ground return of the power supply. This voltage is filtered to eliminate converter switching noise and signal conditioned for telemetry transmission. No provision is made to monitor the ion-pump supply-voltage output.

Telemetry Measurements and Signal Conditioning

Signal conditioning to a standard 0- to 5.0-volt range for all channels is provided by the maser's signal-conditioning subsystem for all payload, spacecraft, and vehicle fourth-stage functions. Telemetry for the fourth-stage accelerometers and pressure gauge is routed through the payload-maser telemetry processor to save the weight and power ordinarily allocated to a dedicated vehicle processor and transmitter.

Signal conditioning for the tank-temperature-monitor thermistor is integral to the thermal-control system, as described earlier. Eight additional temperature-measurement bridges are provided within the signal-conditioning subsystem of the payload maser, seven of which are designed for thermistor sensors at various parts of the payload. The eighth, the antenna-temperature monitor, utilizes a platinum resistance thermistor (RTD). All eight temperature-measurement circuits are physically identical except for the choice of bridge resistances. In each, the thermistor or RTD forms one leg of a resistance bridge. The unbalance voltage, which is a function of the temperature of the sensor, is amplified so that the full temperature range appears as a voltage varying from 0 to +5.0 volts.

The translator/transponder's monitor-channel buffers amplify the static phase error, the automatic gain control (AGC), and the status signals from both the translator and the transponder. These are routine measurements except for the translator AGC, which must be monitored with very high resolution to detect small changes in maser power output. The

translator AGC signal conditioner contains provisions for selecting a small segment of the translator AGC output and expanding this portion to the full 0- to 5.0-volt range. The final adjustment of the translator AGC signal-conditioning circuitry provides a full-scale range from -116 to -110 dbm, established during calibration of the probe maser.

Eight channels of voltage measurements are provided for battery voltage, battery current, and six payload-maser heater voltages.

Three channels for in-flight calibration checks of the telemetry system are included: full scale, +4.980 volts; midscale, +1.00 volts; and ground.

Six measurement channels to monitor maser performance are also incorporated. Two of these monitor the voltage and current of the source RF oscillator. The remaining four — hydrogen pressure, ion-pump current, "atom" level, and "molecule" level — were discussed in previous sections.

The payload-maser signal-conditioning subsystem provides reference voltages and buffer amplifiers for the Scout fourth-stage head pressure gauge. The three Scout fourth-stage accelerometers are internally conditioned; their outputs are routed through the signal conditioner to the telemetry processor.

Telemetry PCM Processor

The telemetry processor is an 8-bit, 37-channel pulse-code-modulated (PCM) system operating at 1000 bps. Each main frame has eight subframes 128 bits in length: 21 providing subframe sync, 3 giving subframe identification (ID), and 104 making up 13 8-bit data words. In turn, four data words are multiplexed, yielding 32 channels per main frame. The remaining five data words are used for high-repetition-rate data as

follows: the translator AGC voltage is sampled once each subframe (eight times each main frame), and the four Scout channels are sampled twice each subframe (16 times for each main frame).

The major components of the telemetry processor consist of an analog-to-digital converter, a main-frame multiplexer, four subframe multiplexers, and a timing and sync generator.

All telemetry-processor circuitry is mounted on eight pie-shaped boards that plug into the electronics ring. The processor's timing circuitry generates the following clock signals for the telemetry system: the bit-rate clock (1000 bps), the coordinate clock (125 bps), and the subframe clock (7.8125 bps). All clocks are derived from, and harmonically related to, the subcarrier oscillator frequency of the transponder's telemetry modulator.

The subcarrier crystal oscillator in the transponder generates a 2.048-MHz signal, which, divided by 2 within the transponder, generates the 1.024-MHz telemetry subcarrier. The 2.048-MHz signal is also routed through the maser/spacecraft interface to the pulse-shaper board, which amplifies the signal and regenerates standard +10-volt COS/MOS logic levels. The 2.048-MHz signal is then digitally divided to 1000 Hz by COS/MOS integrated circuits on the pulse-shaper board. The 1000-Hz clock is routed to the telemetry timing board in the electronics ring.

The pulse shaper contains an auxiliary oscillator operating at approximately 1980 Hz. A clock detector on the pulse shaper detects the absence of an incoming pulse stream from the transponder and automatically switches the auxiliary oscillator on line. The auxiliary oscillator frequency is divided by 2, to 990 Hz, to replace the divided subcarrier oscillator signal for testing or in the event of subcarrier-oscillator failure.

The telemetry timing board, in the electronics ring, consists of several COS/MOS divider chains, delay circuits, and buffer amplifiers, which generate all clock frequencies required for telemetry-system operation. In addition to the major clock signals, the timing board generates a number of auxiliary clocks that are either delayed in time with respect to the main clock or have suppressed pulses for internal system timing applications.

The sync board generates the subframe sync and subframe ID words under control of the timing subsystem. The subframe sync word is a standard Goddard Space Flight Center 21-bit code; the subframe ID is a 3-bit octal word. The subframe sync word is stored in a 21-bit parallel-in, serial-out shift register. The bit pattern is hard-wired into the parallel-input parts. The sync board also accepts data input from the analog-to-digital converter board, assembling the sync word, subframe ID, and data words into a single bit stream at a uniform 1000-bps rate.

The analog-to-digital converter digitizes 0- to +5-volt data into 8-bit data words that are stored in serial-output shift registers. The converter is a completely integrated, 256-level, successive-approximation circuit, requiring 13 digitizing clock cycles for a single digitizing operation. To permit the converter to complete a full cycle of operation in less than eight main-clock cycles, the digitizing clock runs at 32 kbps, derived from the timing-board divider chains. The +4.980-volt reference for the analog-to-digital converter is generated on the source-control/telemetry reference board. The stable +10.0 volts required for operation of this board, in turn, is generated by a separate reference supply, which is installed on the temperature-controlled aft-oven cover.

The main-frame multiplexer accepts 13 analog (0 to +5.0 volts) inputs — four from the subframe multiplexers, one from the translator AGC signal conditioner, and two from each of four Scout measurements — and switches its output to each input in succession. The switching

devices are COS/MOS transmission gates, which are under the control of an on-board counter, and a four- to 16-line converter, which, in turn, is controlled by the timing board.

The subframe multiplexers are mounted on the same circuit boards as the signal-conditioning circuitry. Each subframe multiplexer board contains an eight-channel COS/MOS transmission-gate analog switch and the signal-conditioning circuitry associated with those eight telemetry channels. The transmission gates are controlled by a three- to eight-line digital demultiplexer, which is controlled by the subframe ID-word generator on the sync board.

Pressure and Vehicle Spin-Rate Measurements

Two specialized in-flight measurements are provided for correction of the maser cavity's frequency. The resonant frequency of the maser cavity is a function of the gas pressure within the pressure can, the vehicle spin rate, and the cavity temperature. The last of these is monitored through telemetry by observing the aft-oven-cover heater voltage, but the first two require specific instrumentation provisions.

The sensitivity of maser frequency to pressure within the pressure can is approximately 3.9×10^{-12}/psi. Therefore, a very precise, very high-resolution pressure measurement is required to correct the maser frequency to within $\pm 1 \times 10^{-14}$. This requirement is met by the use of a very stable diaphragm-type pressure transducer and highly stabilized bridge-sensor electronics. The transducer and the electronics package are mounted within the temperature-controlled pressure can at the forward end. Figure 18 is a block diagram of the pressure-measurement assembly.

The pressure transducer, a Bell and Howell type CEC1000, uses thin-film strain gauges and bridge resistors to minimize the differential temperature coefficients of the bridge elements. The bridge excitation

voltage is controlled to within ±10 mvolts to minimize self-heating errors in the bridge balance point. The bridge amplifier, an Analog Devices type AD521S instrumentation amplifier, has a very low-voltage offset coefficient and a high common-mode-rejection ratio. The entire assembly is temperature controlled to better than ±1°C owing to its location within the pressure-can heater system.

The required resolution is obtained by limiting the dynamic range of the measurement to 1.0 psi so as to operate from 17 to 18 psia. In order to obtain 0-volt output from the pressure monitor at 17 psia, it is necessary to offset the bridge amplifier electronically. The effect of changes in the offset voltage on the overall stability of the pressure measurement is minimized by using the bridge excitation voltage as the source of the offset voltage. To first order, changes in the excitation voltage cancel completely at 17 psia and produce only a very small residual error at 18 psia. The resolution of the system, as observed through the 8-bit telemetry system, is approximately 0.004 psi per step of the least-significant digit.

The sensitivity of maser frequency is approximately 1×10^{-14}/rpm at 115 rpm. A very high-resolution spin-rate monitor is therefore required; unfortunately, however, the actual in-flight spin rate cannot be accurately predicted.

The problem of combining high resolution with a wide dynamic range is solved by a sun-sensing dual-resolution monitor that automatically switches from high resolution to a wide-range low-resolution mode for every tenth measurement. A block diagram of this monitor is given in Figure 19. The sun sensor shown in the figure is mounted on the spacecraft honeycomb plate, where it views the sun and the outside world through a small hole in the side of the thermal shield. Each time the vehicle rotation brings the sun into the field of view of the sensor, a pulse is generated, amplified, and used to energize a Schmitt trigger

circuit. A digital division by 2 then generates a gate, the duration of which is equal to the period of the rotation rate; the gate pulse is further divided by 10 to generate a multiple-period gate pulse, which is the average of 10 rotation periods. The multiple-period gate serves two functions: the positive-going edge triggers the sequence control counter, while the pulse opens the main gate, allowing 1000-bps clock pulses to flow to the main counter.

The binary number stored in the 8-bit main counter is a measure of the duration of 20 periods of the vehicle's rotation rate. At the end of each multiple-period gate, a transfer pulse is generated that jam-transfers the contents of the main counter into the storage register and resets the counter to zero. The output of the storage register is the input to an 8-bit digital-to-analog converter, identical to the one used in the telemetry processor's analog-to-digital converter. The analog output of this converter is amplified and routed to the appropriate telemetry subcarrier multiplexer for processing.

The main counter's most-significant digit frequently overflows during a high-resolution measurement cycle, resulting in an ambiguity regarding the absolute value of the measured spin rate; the full-scale range of the sensor is approximately 6 rpm within the range centered near 114 rpm, i.e., 111.61 to 117.19 rpm. To resolve this ambiguity, the sequence switches the clock pulses through a divide-by-10 for one measurement cycle after every 10 high-resolution measurement cycles. The unambiguous range of the sensor is much larger at the lower clock rate than at the higher rate, thus making it possible, by using both sets of data, to determine the rotation rate of the vehicle.

Since the payload's telemetry processor has no provision for direct entry of digital data, it is necessary to convert the digital rotation-period data to analog form and redigitize them in the telemetry processor. The error buildup that might be inherent in such a process is

minimized by using a small full-scale range, a precise reference derived from the telemetry reference board for the digital-to-analog-converter reference voltage, and the crystal-controlled subcarrier oscillator as the source of the 1000-Hz main counter clock.

As noted earlier, the spin sensor is mounted on the spacecraft's main honeycomb plate and is thus the only component of the maser electronics system that is not physically installed on the maser itself. The resolution of the spin sensor, in its design range, is approximately $\pm$0.02 rpm; the estimated overall accuracy is approximately 0.05 rpm, including the quantizing error.

Payload Ground Support Electronics Equipment

Two major items of equipment are required for direct support of the payload maser during qualification tests and on the pad before launch; these are the payload control rack and the SAO frequency standard, both of which are installed in the support trailer used for normal operations. The payload control rack houses facilities for operating the relays in the payload for field, source, and cavity during control, for decoding spacecraft telemetry, and for displaying quick-look digital and analog data of selected telemetry channels. The frequency standard provides facilities for measuring the frequency stability of the payload maser at the output frequency of the translator, 2203.078 MHz.

Figure 20 is a photograph of the payload control rack. The three functional groups within the rack are the Zeeman-frequency audio oscillator, the controller group, and the quick-look telemetry group. The magnetic field within the maser cavity can be measured by applying an audio-frequency field across the cavity structure and observing the frequency at which the maser output level dips (nominally between 500 and 1000 Hz) owing to Zeeman transitions induced between the $M_F = \pm 1$ and

0 sublevels of the upper energy state of the hydrogen atom. The audio-frequency source in the payload control rack is a Hewlett-Packard Model 651B audio oscillator. A printed-circuit loop on the vacuum tank is wired to the oscillator output through the umbilical cable.

Payload Controls

The magnetic-latching relays in the payload are controlled by push-button switches on the payload control rack, each switch controlling one relay in a binary sequence. The six sets of push-button controls comprise three for the magnetic fields, one for cavity tuning, one for hydrogen pressure, and one for source oscillator voltage.

The extremely simple relay-control circuitry is designed to avoid spurious relay operation caused by power failure or electronic malfunction and to provide nonvolatile memory between times when the payload is energized. The operator presets the desired binary number into push buttons for a particular function. A green indicator lamp in the bottom half of each preset button indicates which switches have been depressed; no power can be applied to the relays at this point. After the preset number has been verified, the operator momentarily depresses the set switch to apply power to the relay coils. A red indicator lamp in the top half of each preset switch signals when the set control is operating properly.

The relays can be energized from the power supply on the payload control rack only if the set switch is depressed; otherwise, the relay coils are completely disconnected from the GSEE. Each relay coil line is brought out individually, through the umbilical cable, to the control rack without involving the spacecraft electronics in any way; thus, no malfunction aboard the spacecraft can alter the state of the relays once they are set from the GSEE payload control rack.

Quick-Look Telemetry

The control rack houses a Coded Communications Corp. Model ECO-1 PCM decoder, a digital-display unit, and an analog-display unit.

The decoder accepts the payload's PCM bit stream and a 1000-bps clock. Both signals are provided by special balanced line drivers on the maser payload and are routed through the umbilical cable to balanced line receivers in the payload control rack and then to the input of the PCM decoder. The balanced signal lines enhance the common-mode noise rejection of the quick-look telemetry system and also preserve the ground isolation of the payload electronics. The output of the PCM decoder is a parallel 8-bit natural binary data word, a 6-bit parallel word ID, and a 3-bit subframe ID. The decoder output cycles through all 218 8-bit main-frame words in 1.024 sec; each word is identified by the appropriate word and subframe IDs.

The data bus, the word ID bus, and the subframe ID bus are routed to the digital-display unit. The system also provides for selective digital-to-analog conversion on four channels for real-time monitoring on strip-chart recorders.

CONCLUSIONS

At the time of writing this paper, the data-reduction phase of the experiment is in full swing. The reduction process consists of comparing the frequency of the relativity signal obtained from the system shown in Figure 1 with predictions of what this signal frequency should be from currently accepted relativity theory. The input data for the predictions depend on tracking the position and velocity of the probe to very high accuracy and deriving from these data the relativistic frequency predictions, including redshift, second-order doppler, and earth-motion effects. From the data processing, still in progress, we

can recover the Allan variance of the output data taken at maximum range, shown in Figure 21. These data include the effects of more than 30000 km of propagation and three passes through the earth's atmosphere and ionosphere. These data are quite similar to maser-comparison data taken in the laboratory over a few meters of cable!

For the longer term data taken during the mission, Figure 22 shows the residual frequency between observation and predictions based on a preliminary trajectory determination. The discrepancies near the ends are still not understood in detail; however, in the present analysis of the tracking data used in determining the trajectory, there appears to be an incorrect representation of the payload's dynamics during the flight, and a more complete computation is required to obtain the probe's trajectory. We look forward to presenting a total picture of the outcome of this experiment in the near future.

ACKNOWLEDGMENT

This work was supported in part by Contract NAS8-27969 from the National Aeronautics and Space Administration.

REFERENCES

1. R. F. C. Vessot and M. W. Levine, Performance data of space and ground hydrogen masers and ionospheric studies for high accuracy comparisons between space and ground clocks. In Proceedings of the 28th Annual Frequency Control Symposium, U.S. Army Electronics Command, Ft. Monmouth, N.J., pp. 408-414, 1974.
2. D. Kleppner, R. F. C. Vessot, and N. Ramsey, The orbiting clock experiment to determine the gravitational redshift. Astrophys. Space Sci., vol. 6, pp. 13-32, 1970.

3. R. F. C. Vessot and M. W. Levine, Measurement of the gravitational redshift using a clock in an orbiting satellite. In Proceedings of the Conference on Experimental Tests of Gravitation Theories, ed. by R. W. Davies, Jet Propulsion Lab. Rep. 33-499, pp. 54-64, 1971.
4. R. F. C. Vessot, Lectures on frequency stability and clocks and on the gravitational redshift experiment. In Experimental Gravitation, ed. by B. Bertotti, Academic Press, New York, pp. 111-162, 1974.
5. S. Petty, R. Sydnor, and P. Dachel, Hydrogen maser frequency standards for the deep space network. In Proceedings of the Eighth Annual Precise Time and Time Interval Applications and Planning Meeting, U.S. Naval Research Laboratory (this volume).
6. M. W. Levine, R. F. C. Vessot, E. M. Mattison, E. Blomberg, T. E. Hoffman, G. Nystrom, D. F. Graveline, R. L. Nicoll, C. Dovidio, and W. Brymer, A hydrogen maser design for ground applications. In Proceedings of the Eighth Annual Precise Time and Time Interval Applications and Planning Meeting, U.S. Naval Research Laboratory (this volume).

FIGURE CAPTIONS

Fig. 1 — Doppler canceling system.

Fig. 2 — Schematic of the cavity support system.

Fig. 3 — Cavity components.

Fig. 4 — Probe-maser thermal-control system.

Fig. 5 — Magnetic shields and insulation.

Fig. 6 — Redesign of external magnetic shield showing the effect of stress.

Fig. 7 — Control electronics located on the aft-oven cover.

Fig. 8 — Two-sided printed-circuit C-field solenoid.

Fig. 9 — Main mounting frame with electronics bays.

Fig. 10 — Aft vacuum manifold assembly.

Fig. 11 — SAES Sorbac cartridge used for hydrogen scavenging.

Fig. 12 — RF dissociator and hydrogen system.

Fig. 13 — Payload assembly.

Fig. 14 — Block diagram of the probe-maser electronics assembly.

Fig. 15 — Block diagram of a typical controller.

Fig. 16 — Typical electronics board.

Fig. 17 — Cavity electronics tuning system.

Fig. 18 — Block diagram of the pressure transducer assembly.

Fig. 19 — Block diagram of the dual-resolution payload spin sensor.

Fig. 20 — Payload-maser ground support control rack.

Fig. 21 — Allan variance of the redshift beat frequency near apogee, taken from the system shown in Fig. 1.

Fig. 22 — Data from the preliminary payload trajectory.

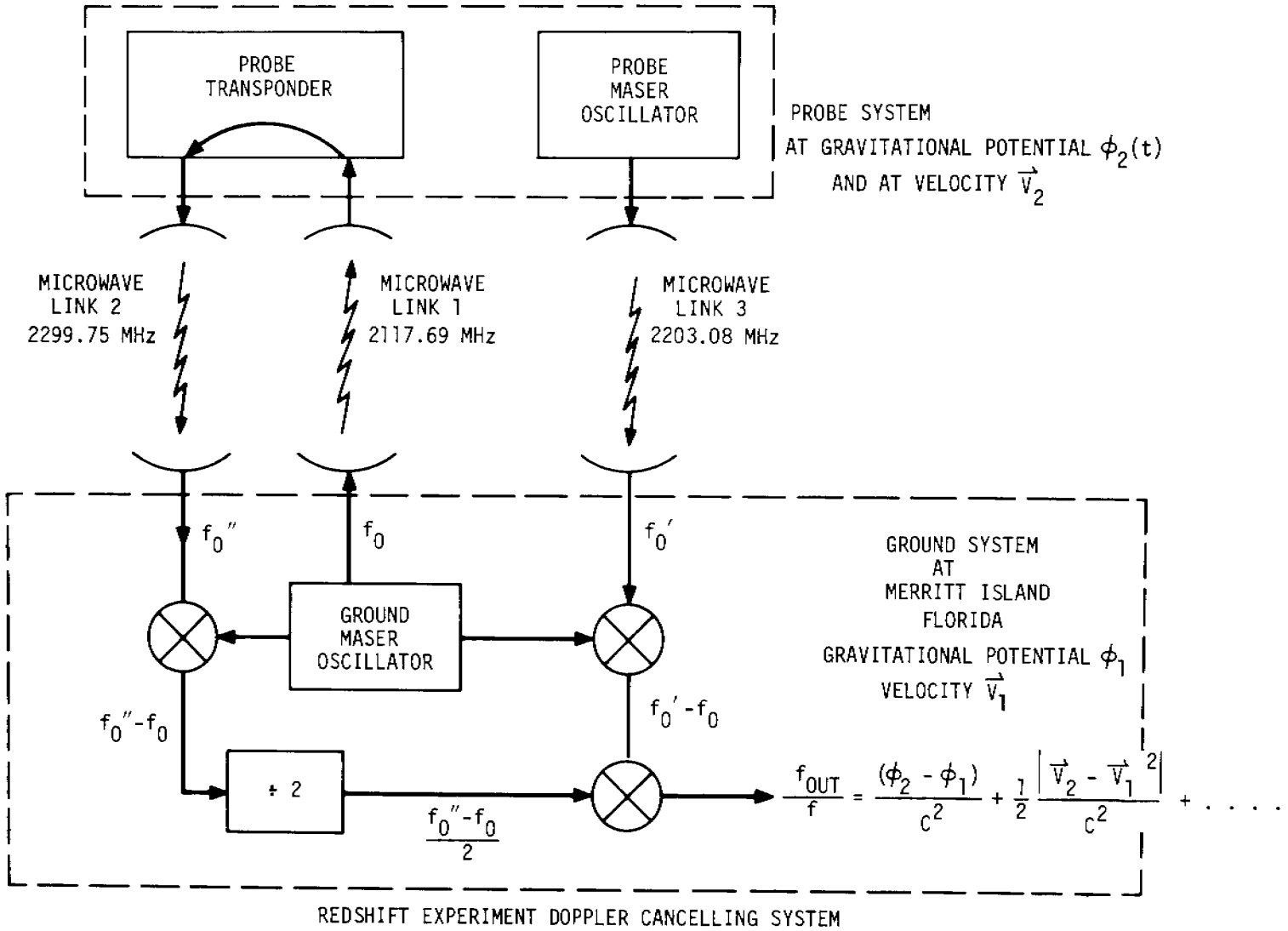

Fig. 1 Doppler cancelling system.

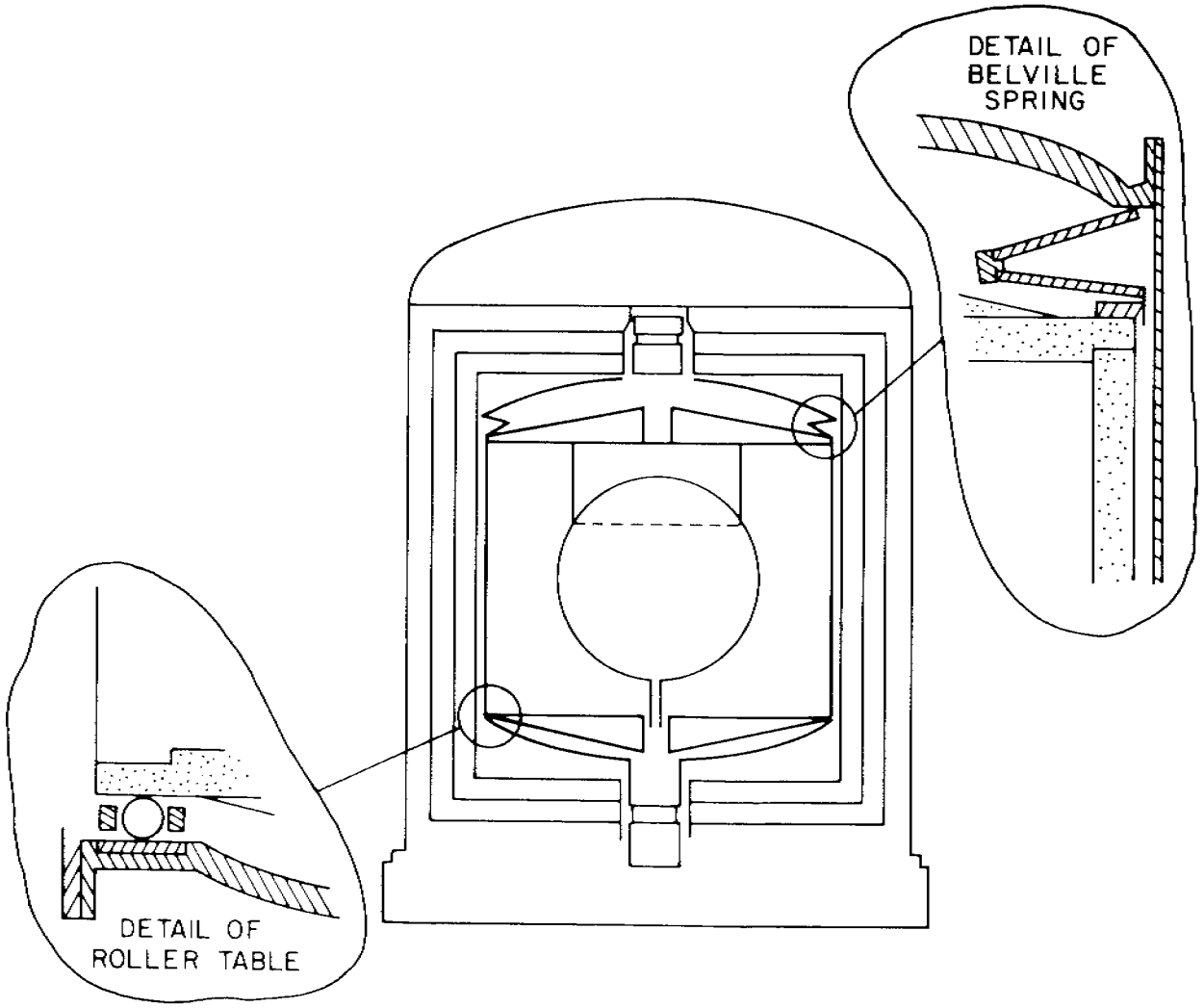

Fig. 2 Schematic of the cavity support system.

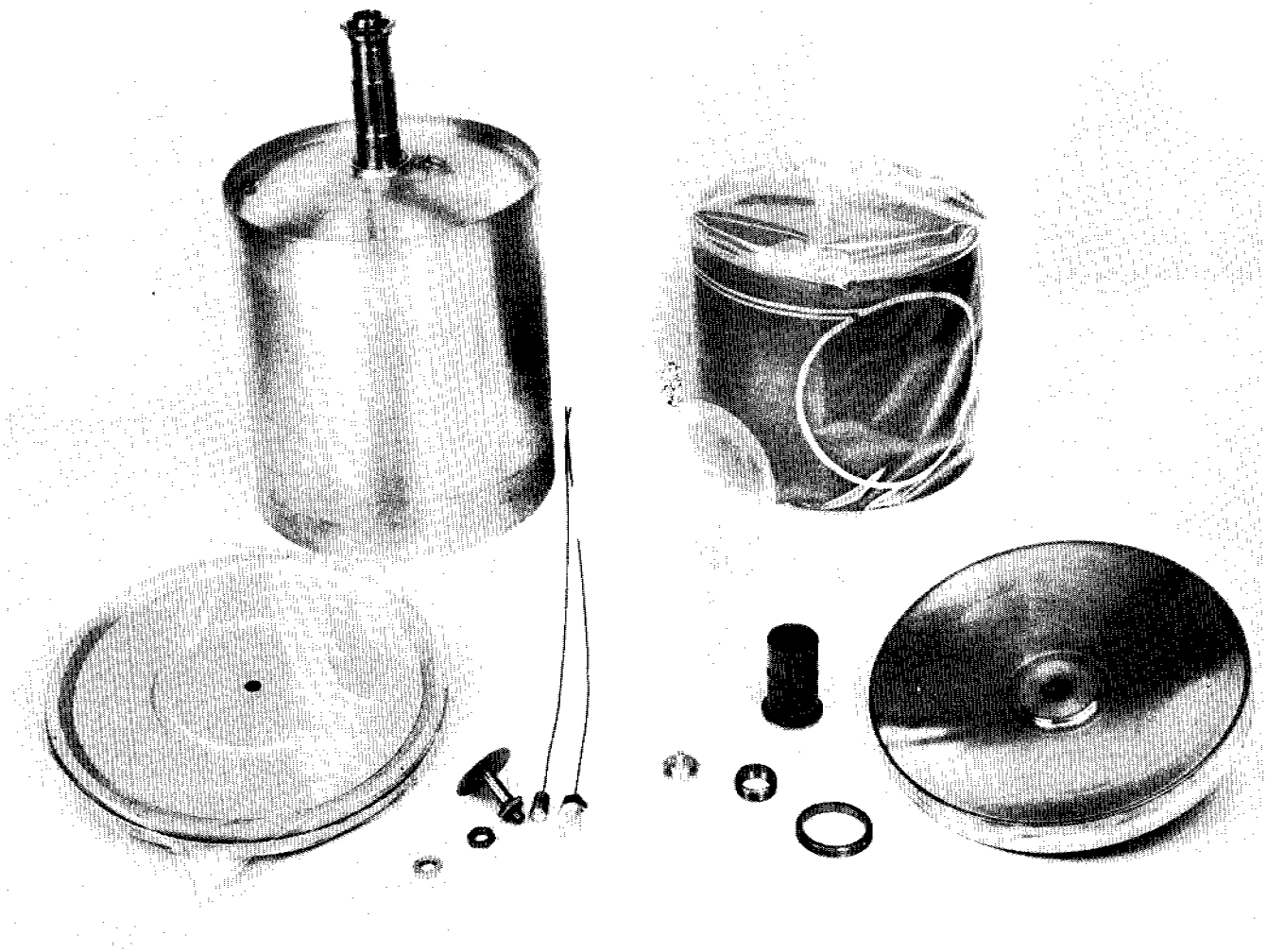

Fig. 3 Cavity components.

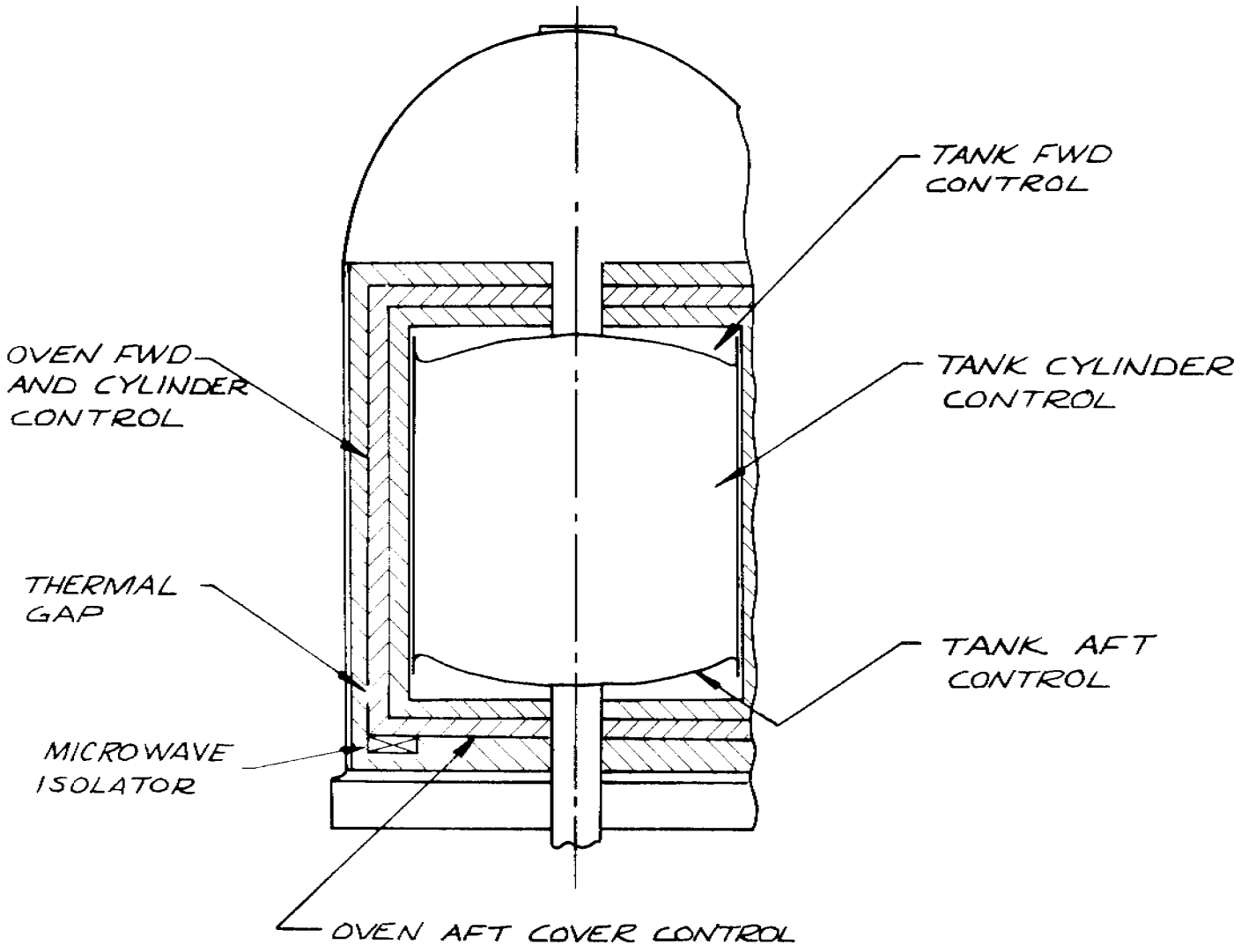

Fig. 4 Probe-maser thermal-control system.

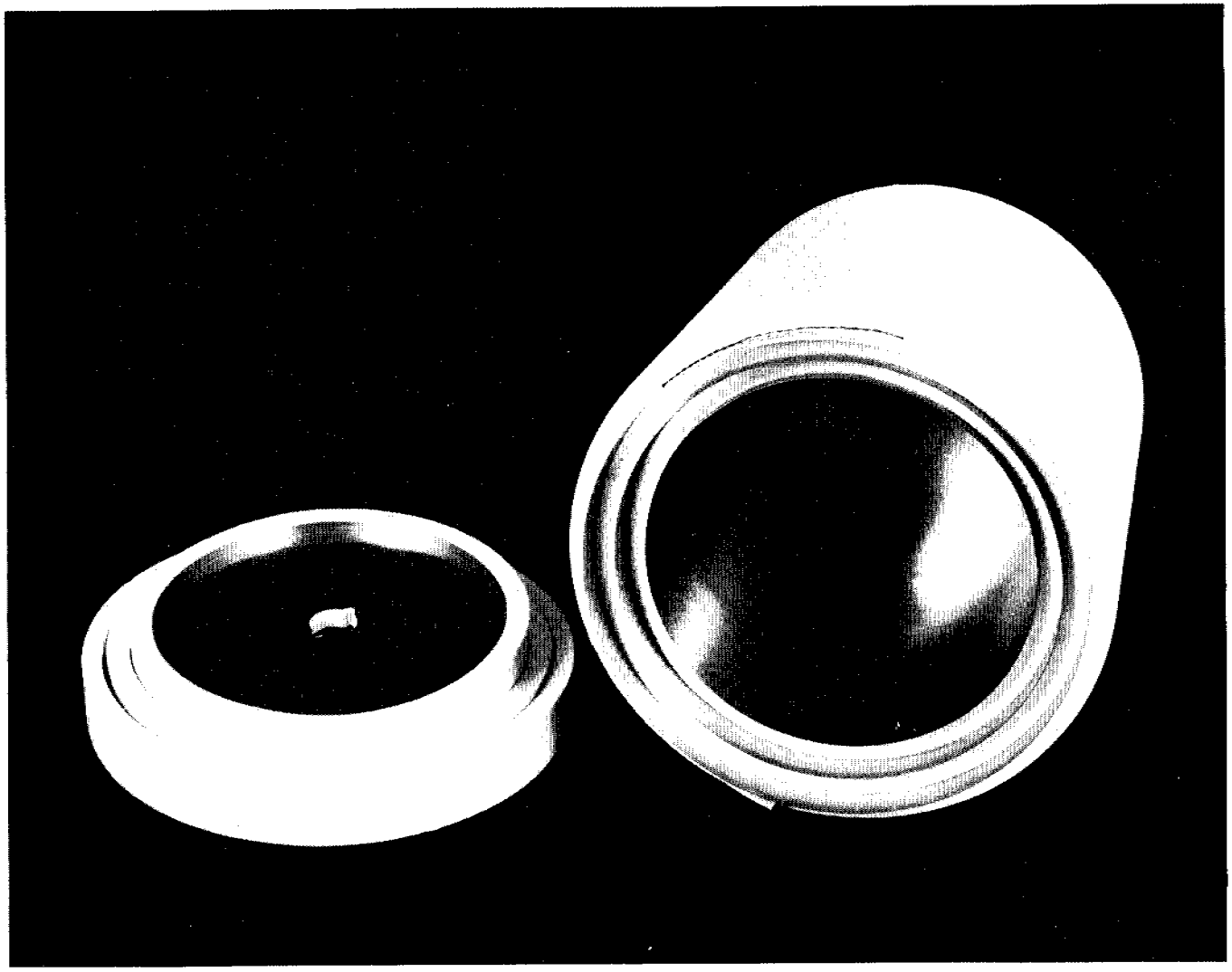

Fig. 5 Magnetic shields and insulation.

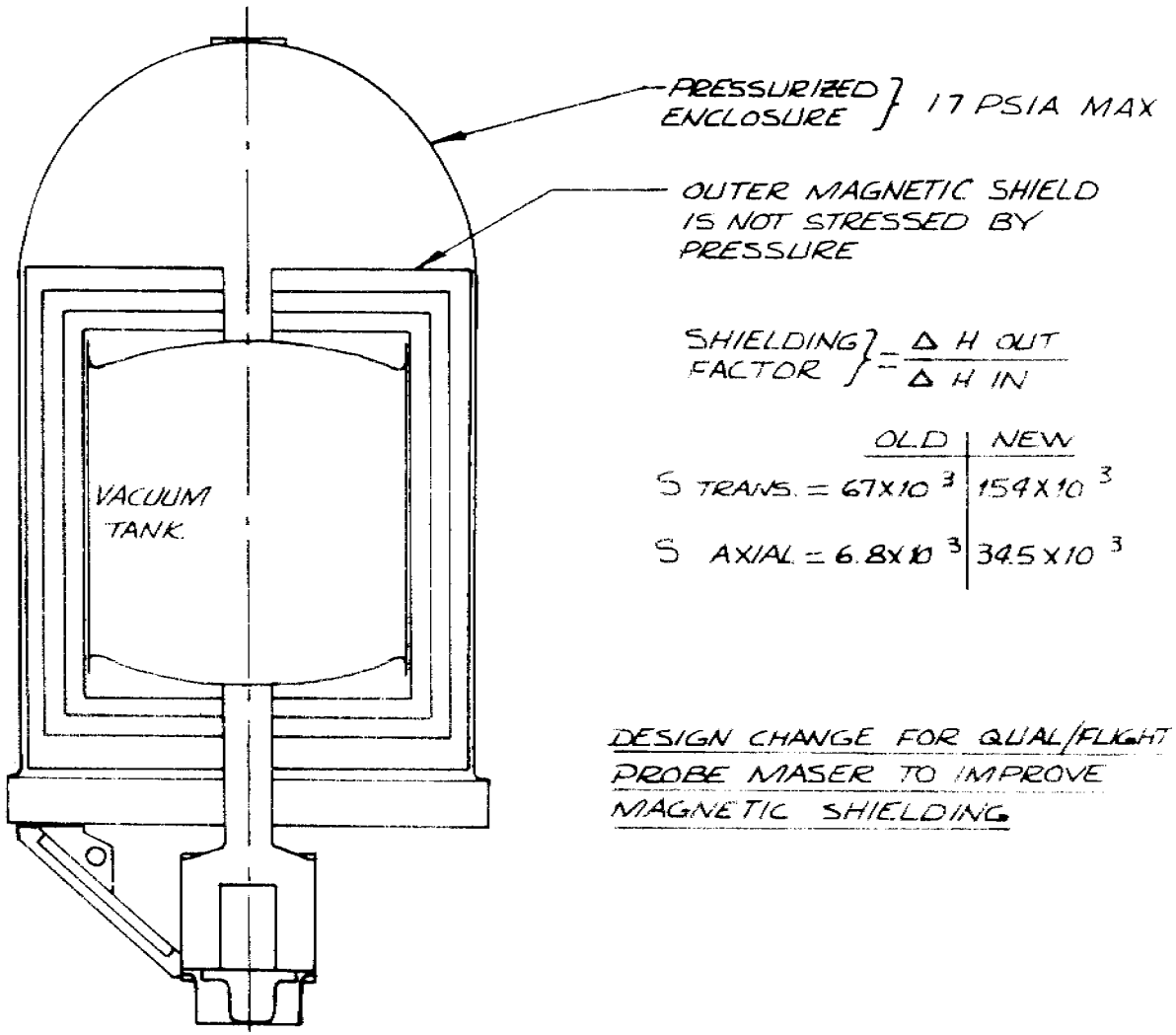

Fig. 6 Redesign of external magnetic shield showing the effect of stress.

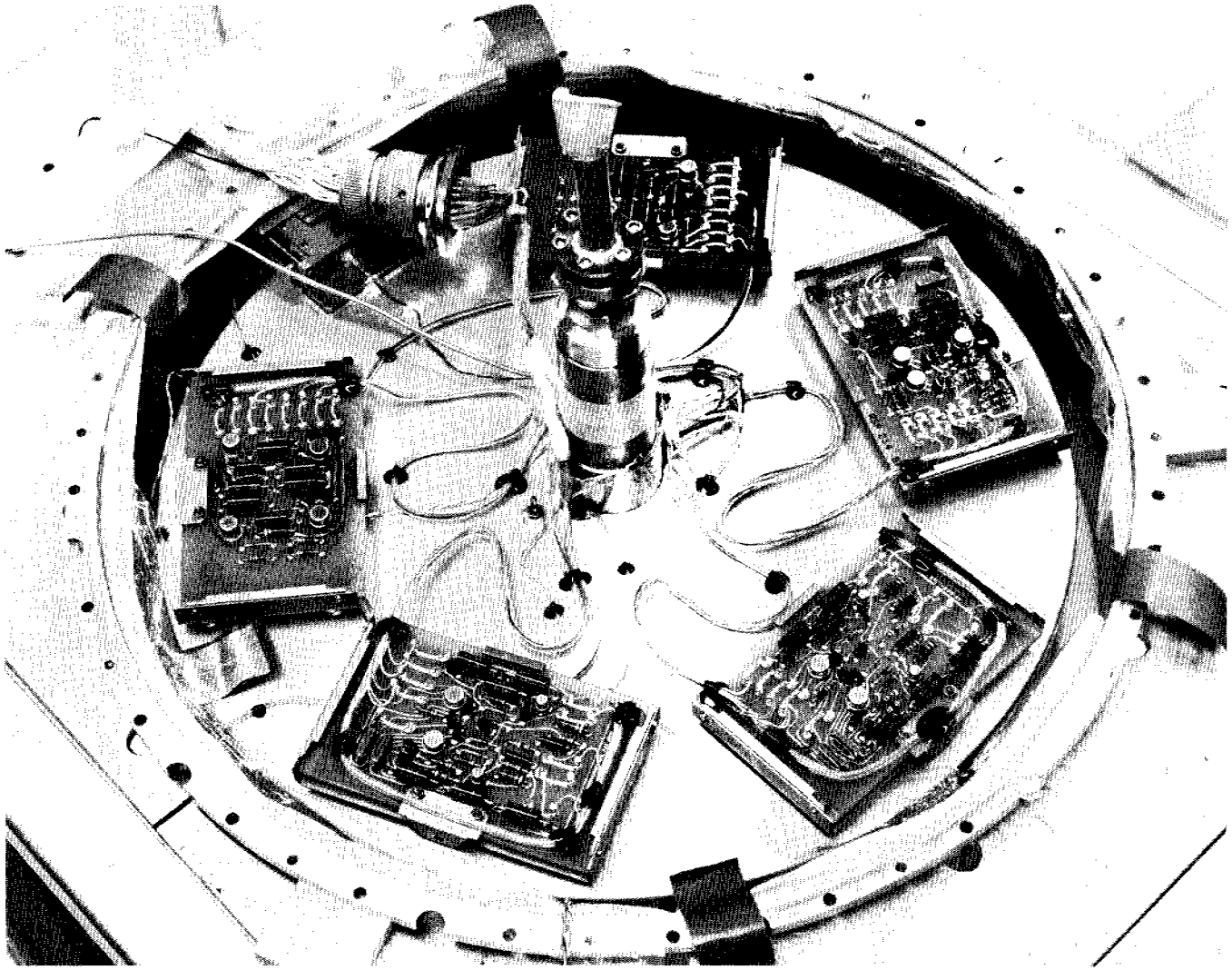

Fig. 7 Control electronics located on the aft-oven cover.

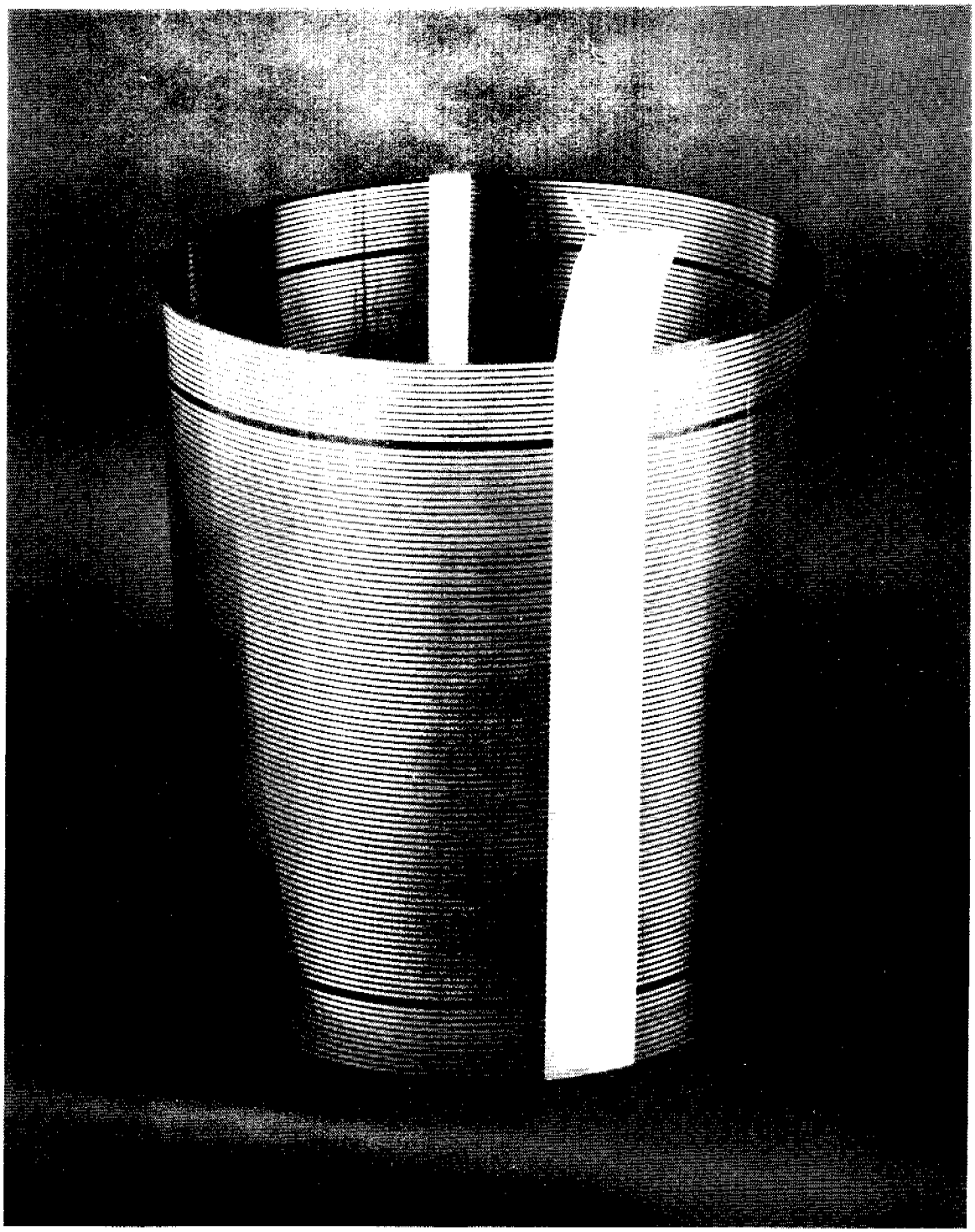

Fig. 8 Two-sided printed-circuit C-field solenoid.

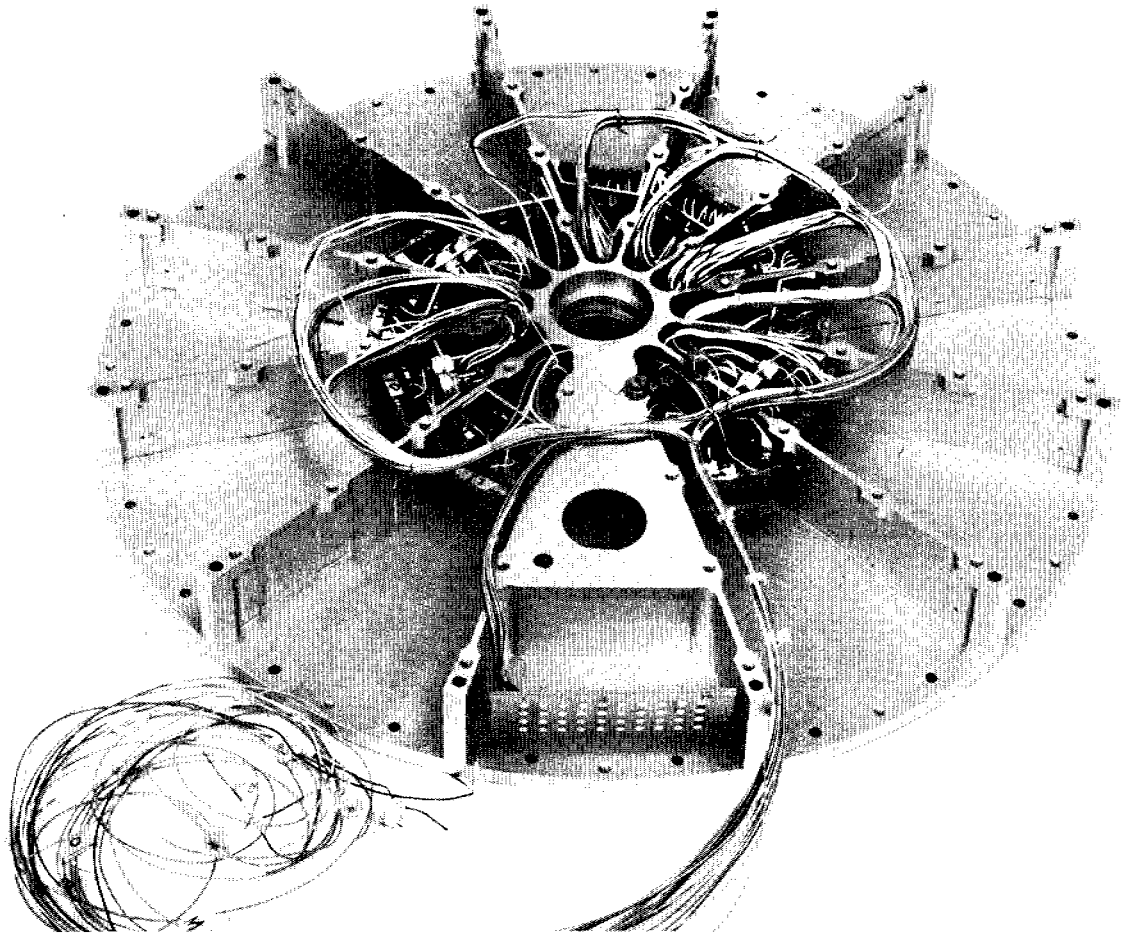

Fig. 9 Main mounting frame with electronics bays.

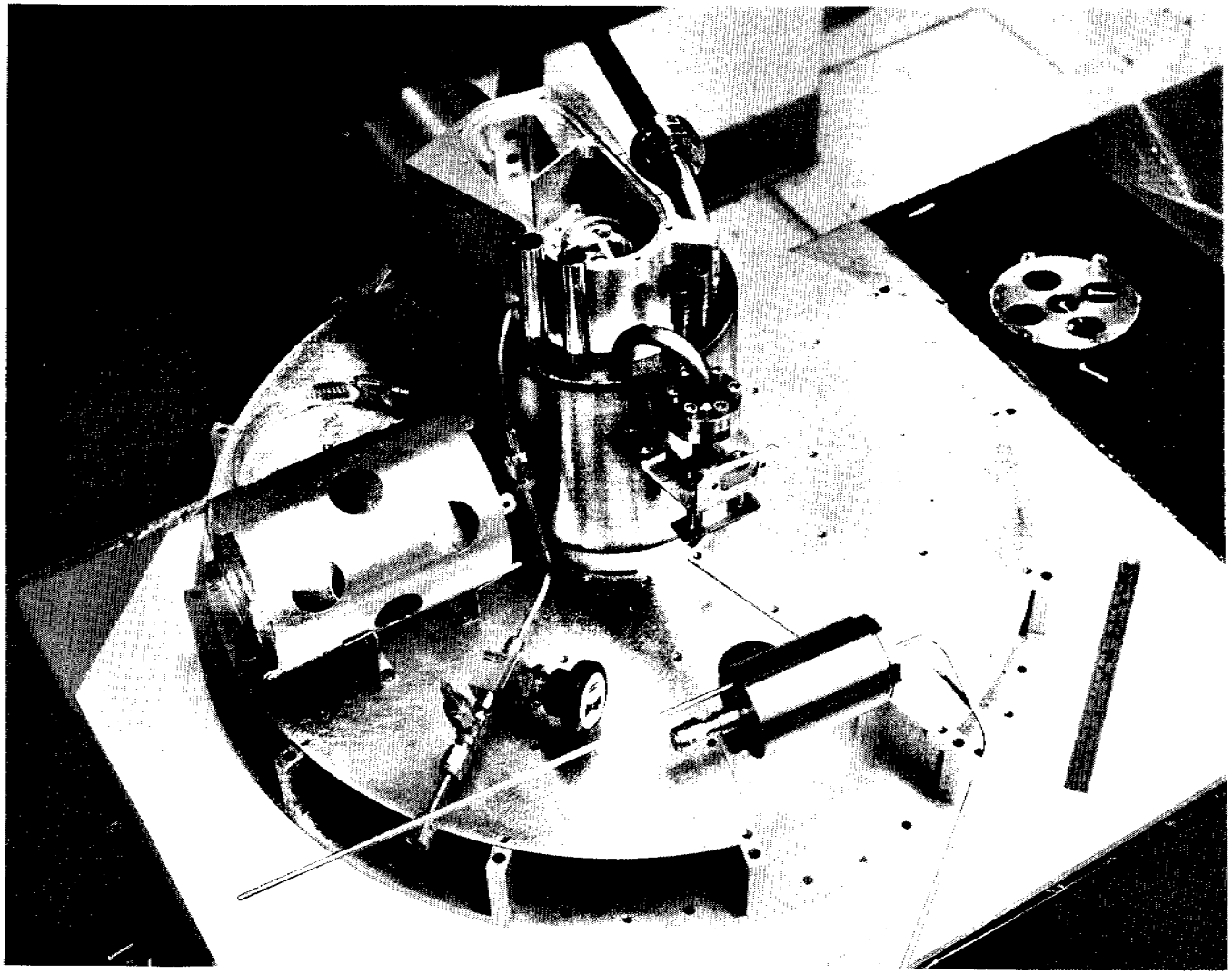

Fig. 10 Aft vacuum manifold assembly.

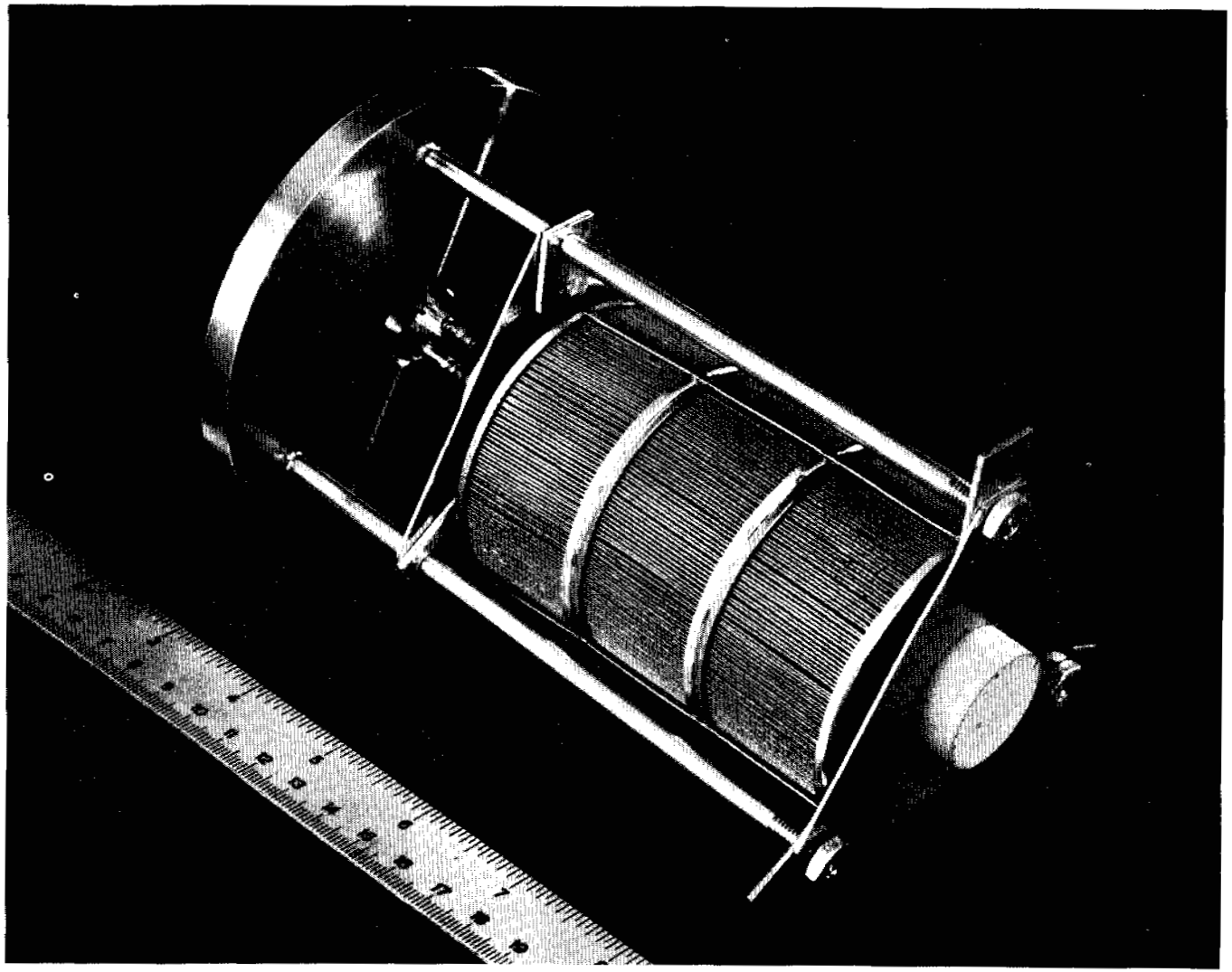

Fig. 11 SAES Sorbac cartridge used for hydrogen scavenging.

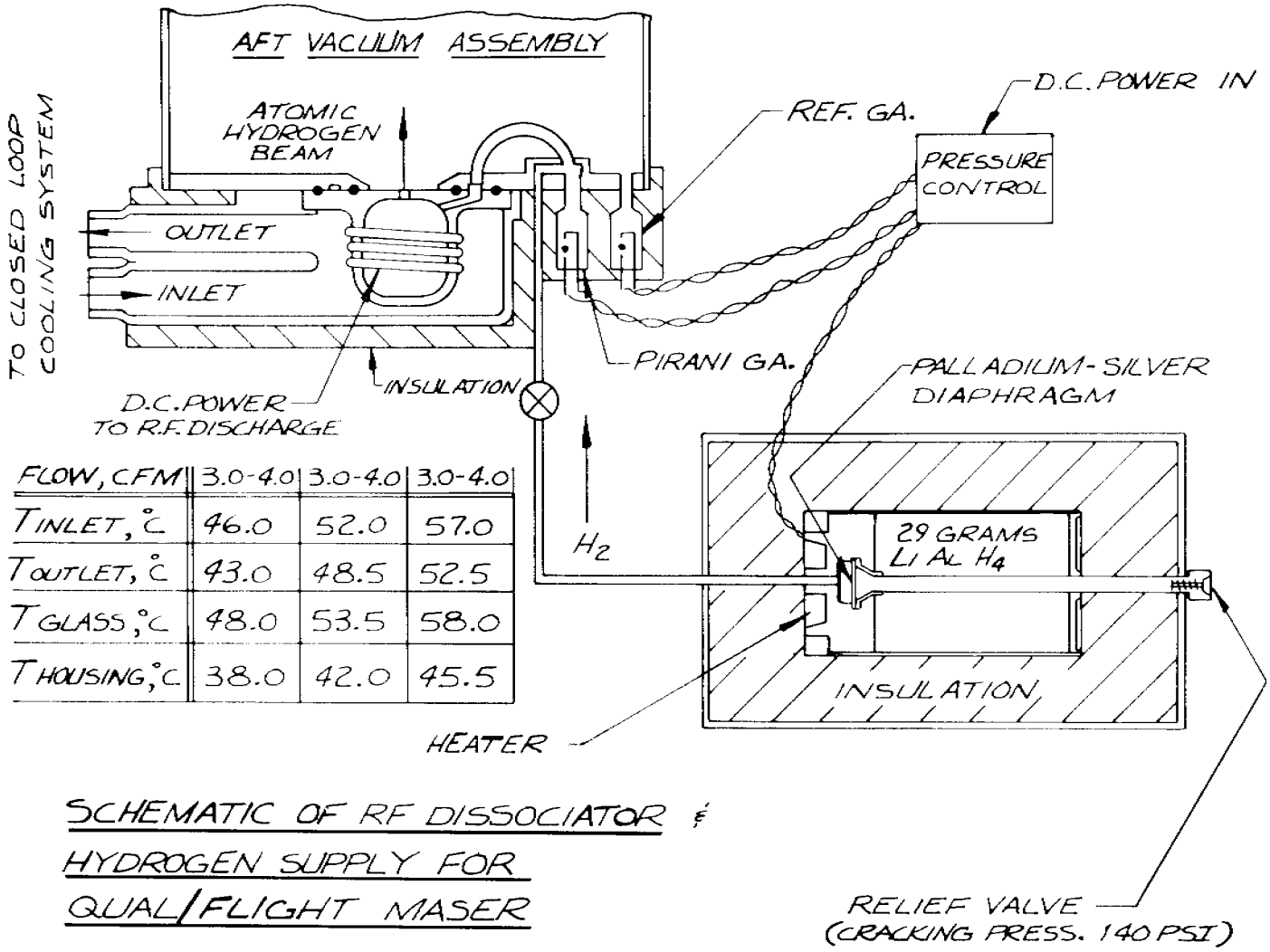

FLOW, CFM	3.0-4.0	3.0-4.0	3.0-4.0
T_{INLET}, °C	46.0	52.0	57.0
T_{OUTLET}, °C	43.0	48.5	52.5
T_{GLASS}, °C	48.0	53.5	58.0
$T_{HOUSING}$, °C	38.0	42.0	45.5

SCHEMATIC OF RF DISSOCIATOR & HYDROGEN SUPPLY FOR QUAL/FLIGHT MASER

Fig. 12 RF dissociator and hydrogen system.

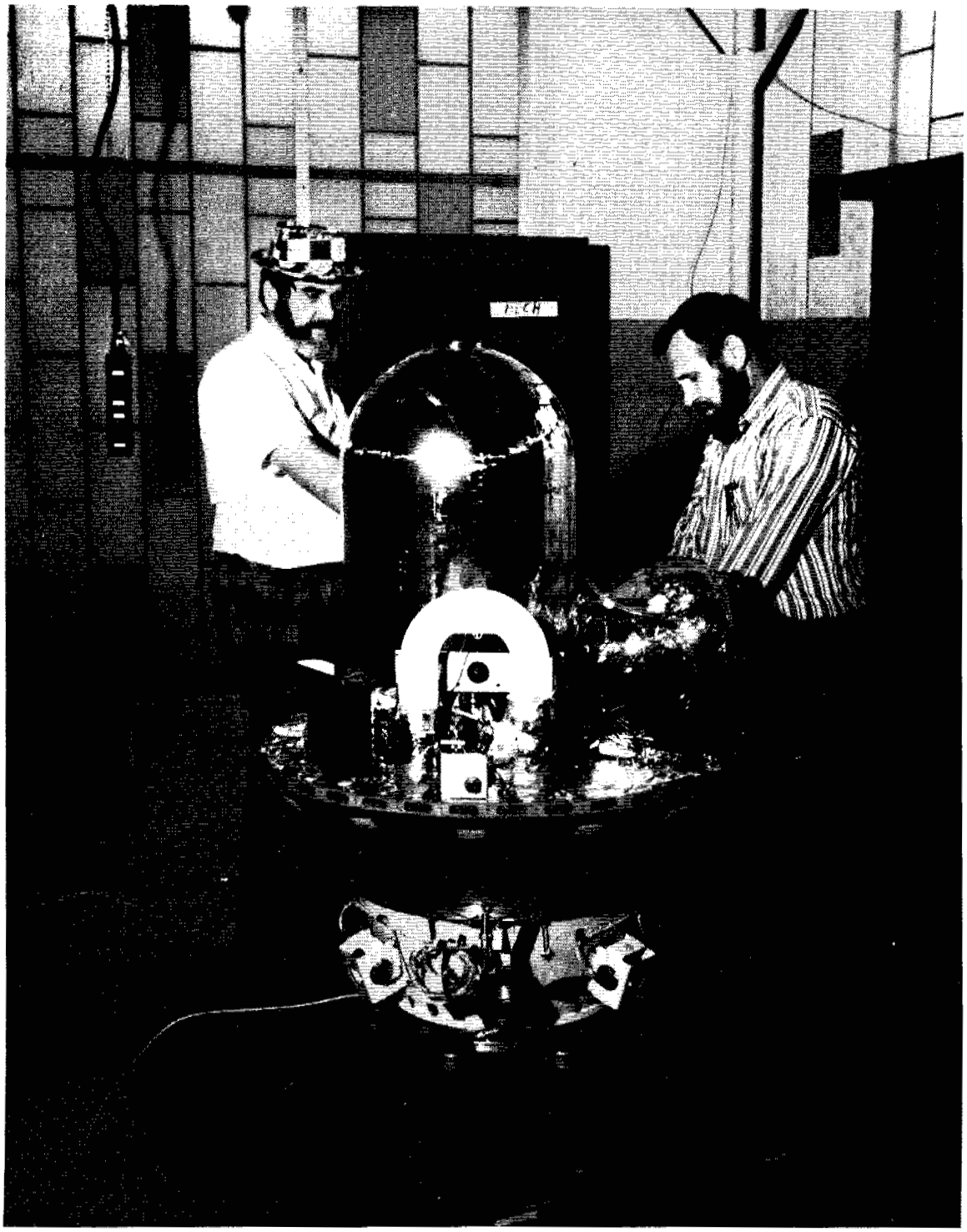

Fig. 13 Payload assembly.

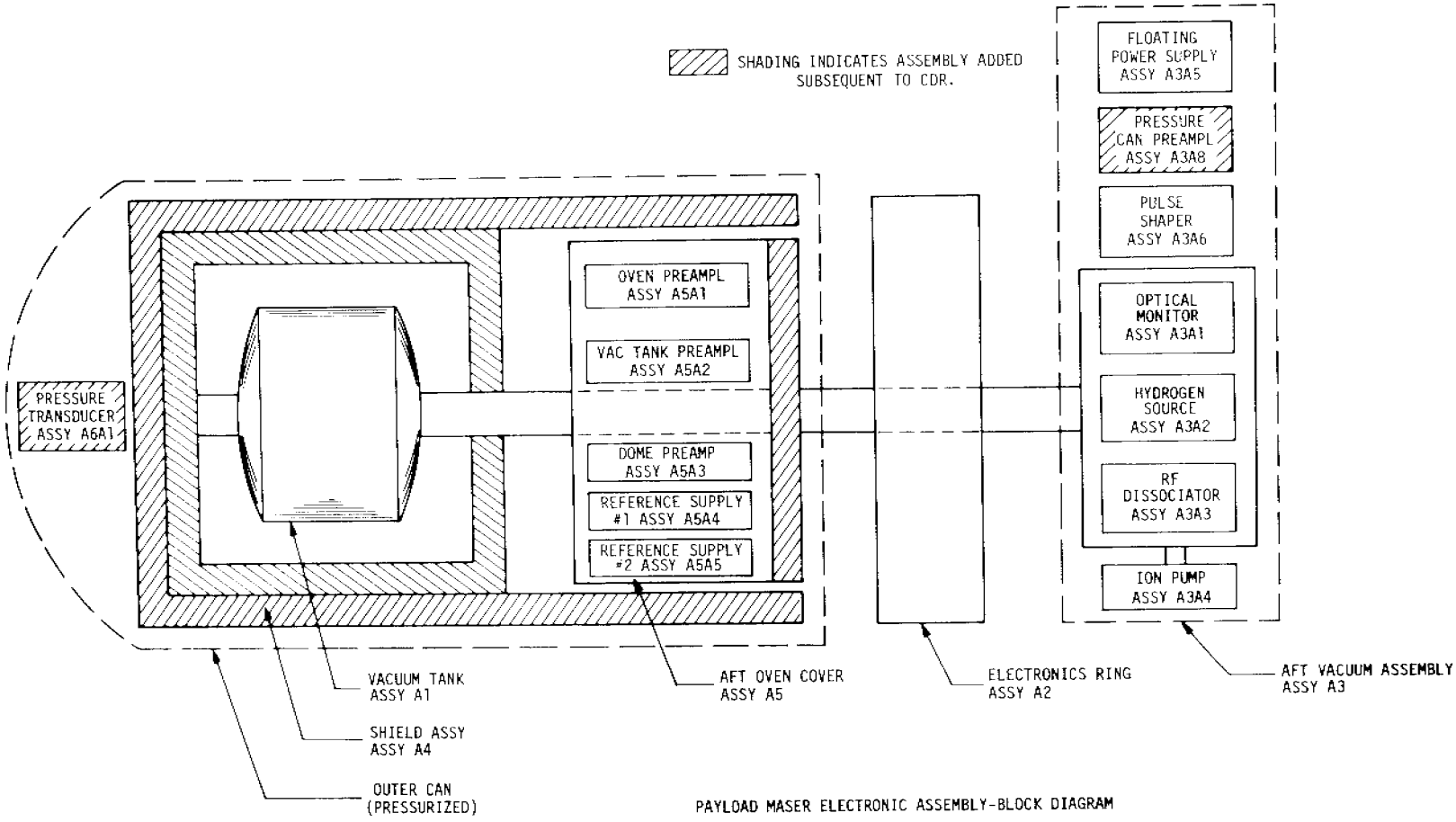

Fig. 14 Block diagram of the probe-maser electronics assembly.

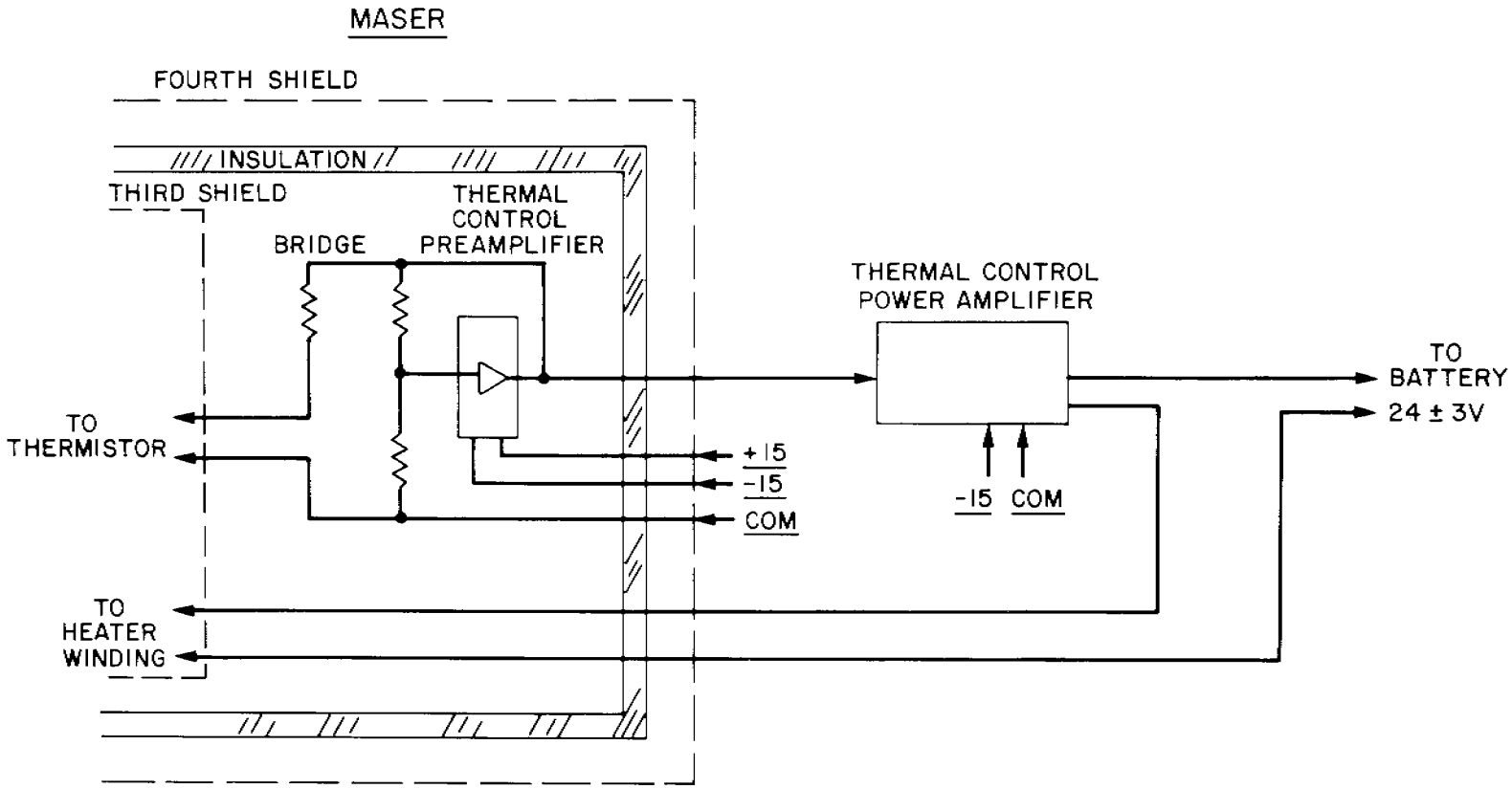

THERMAL CONTROLLERS BLOCK DIAGRAM

Fig. 15 Block diagram of a typical controller.

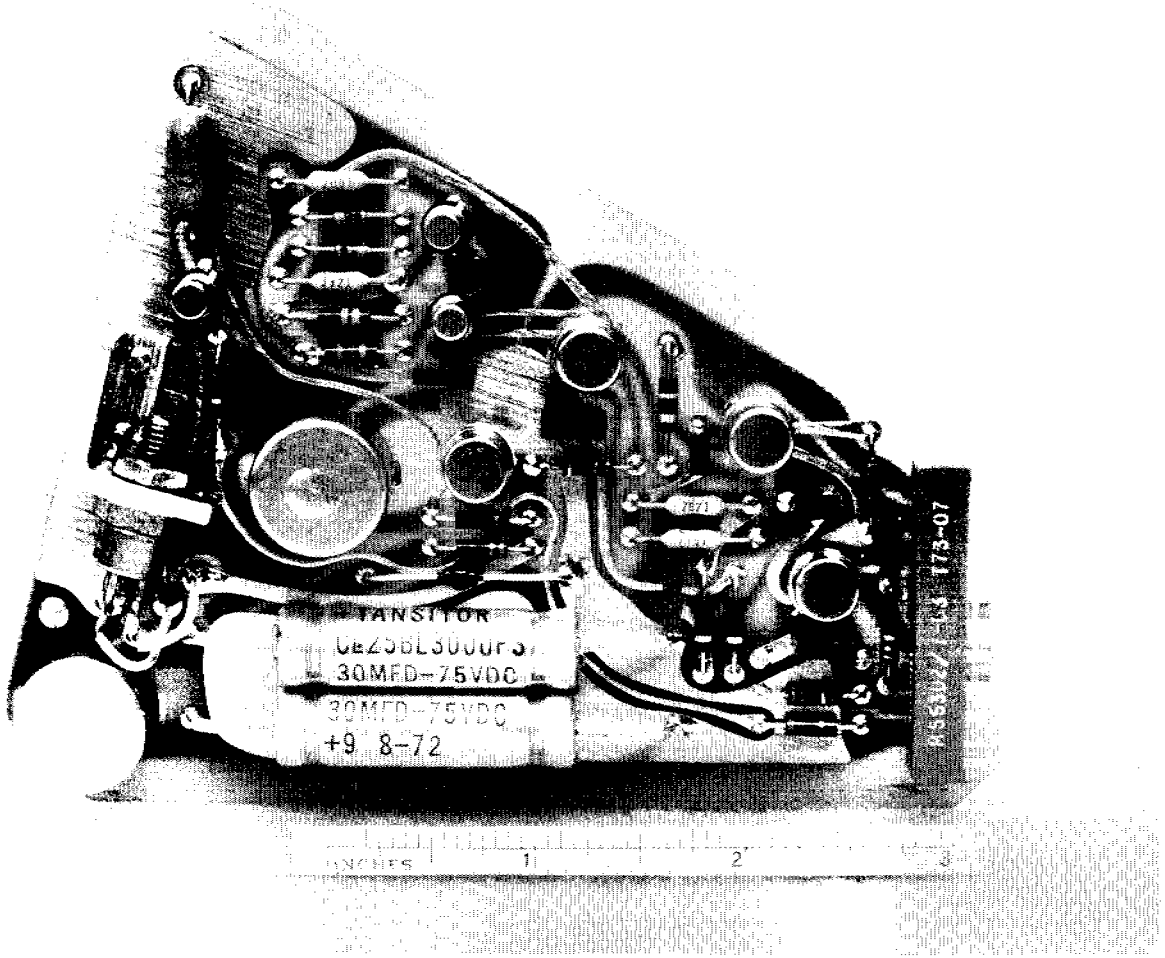

Fig. 16 Typical electronics board.

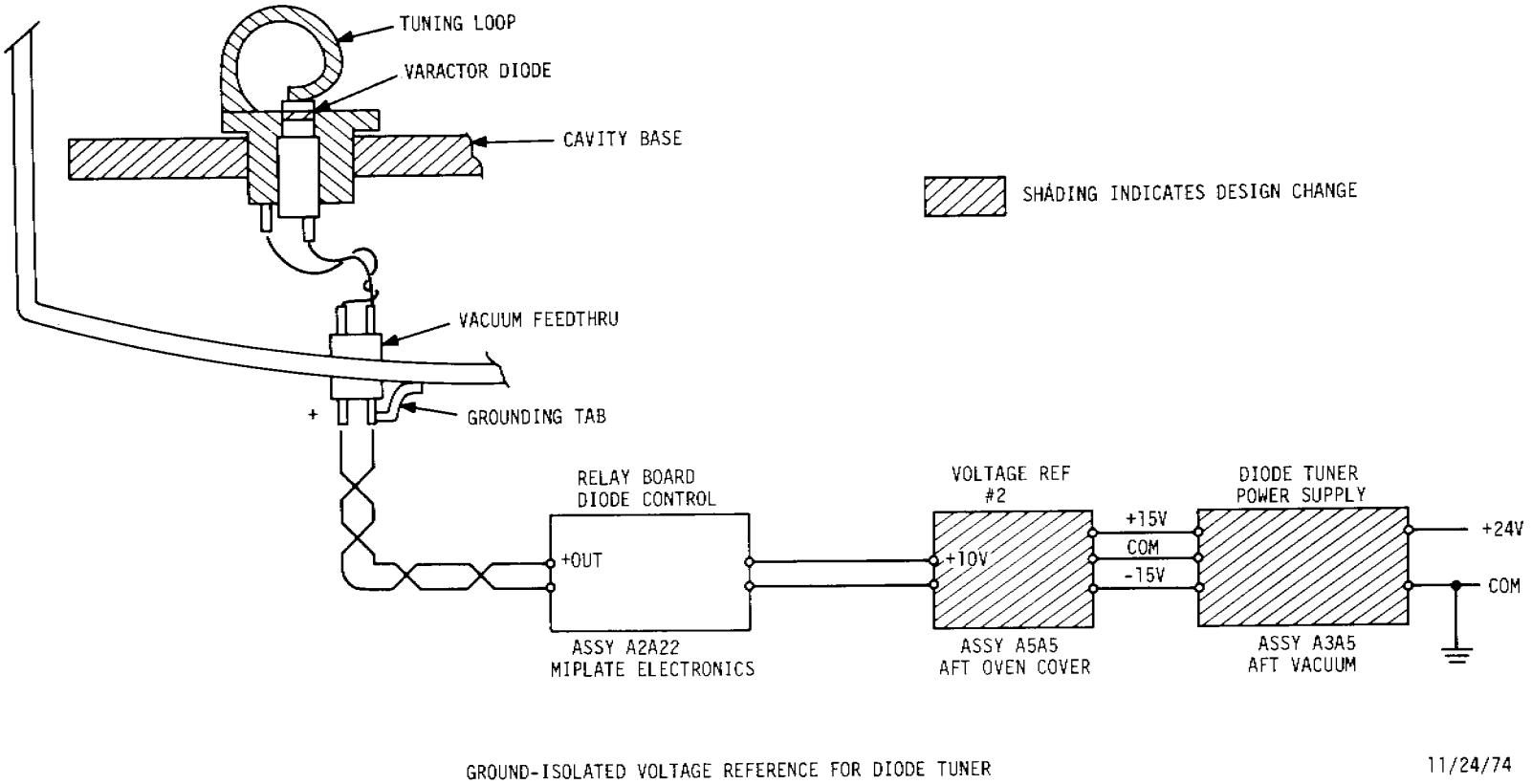

Fig. 17 Cavity electronics tuning system.

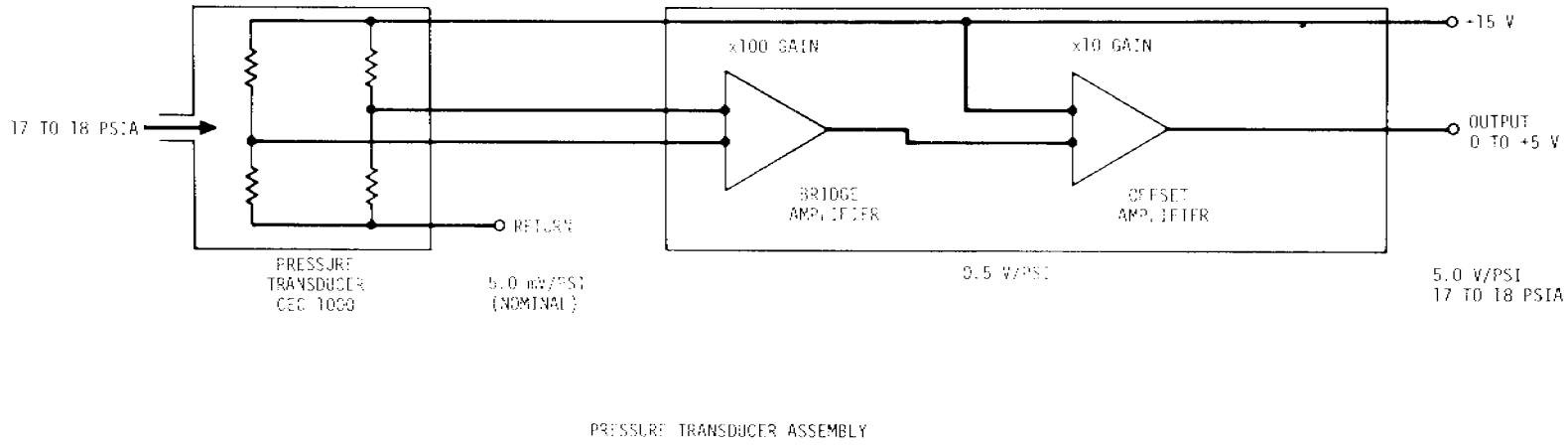

Fig. 18 Block diagram of the pressure transducer assembly.

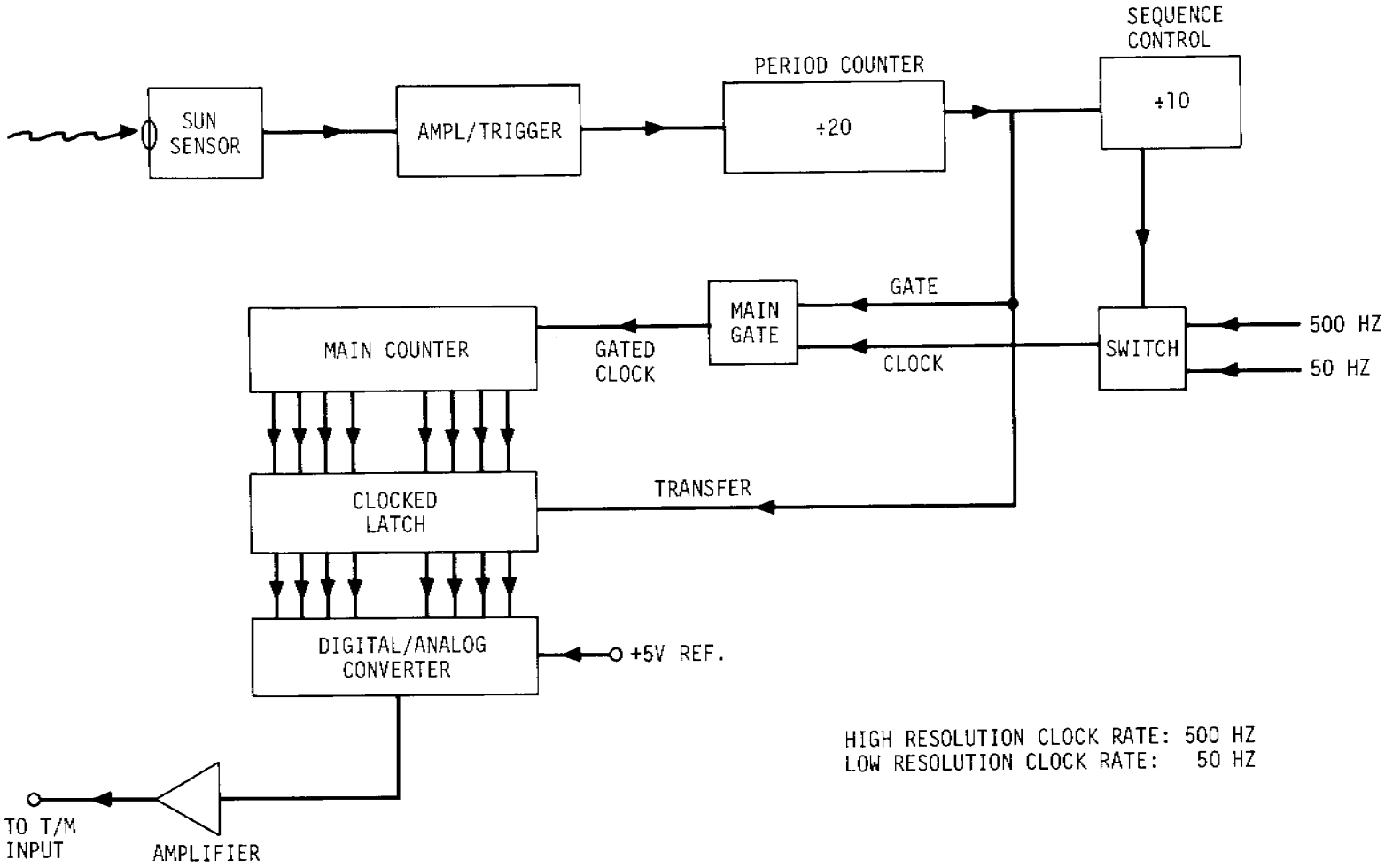

Fig. 19 Block diagram of the dual-resolution payload spin sensor.

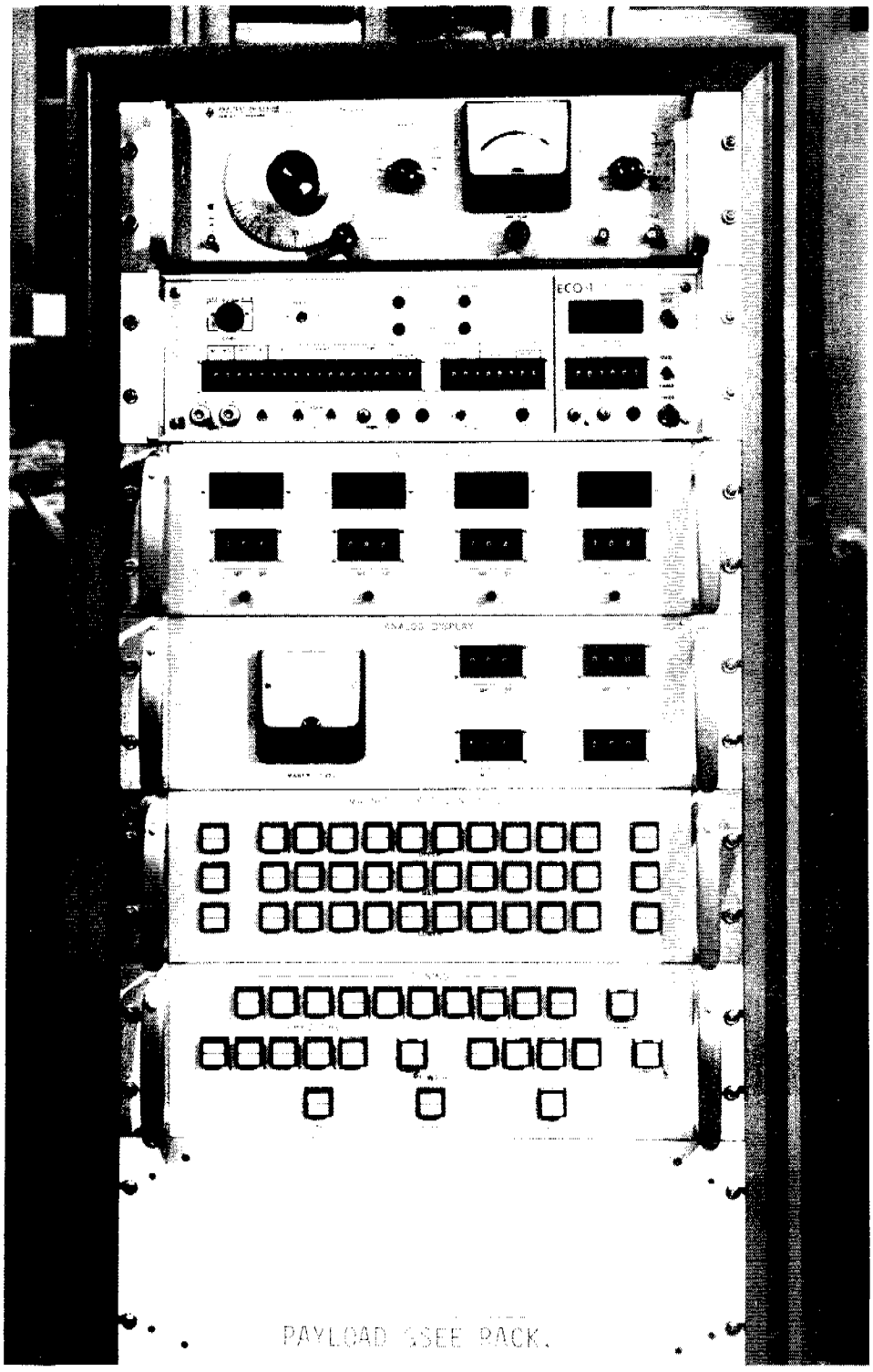

Fig. 20 Payload-maser ground support control rack.

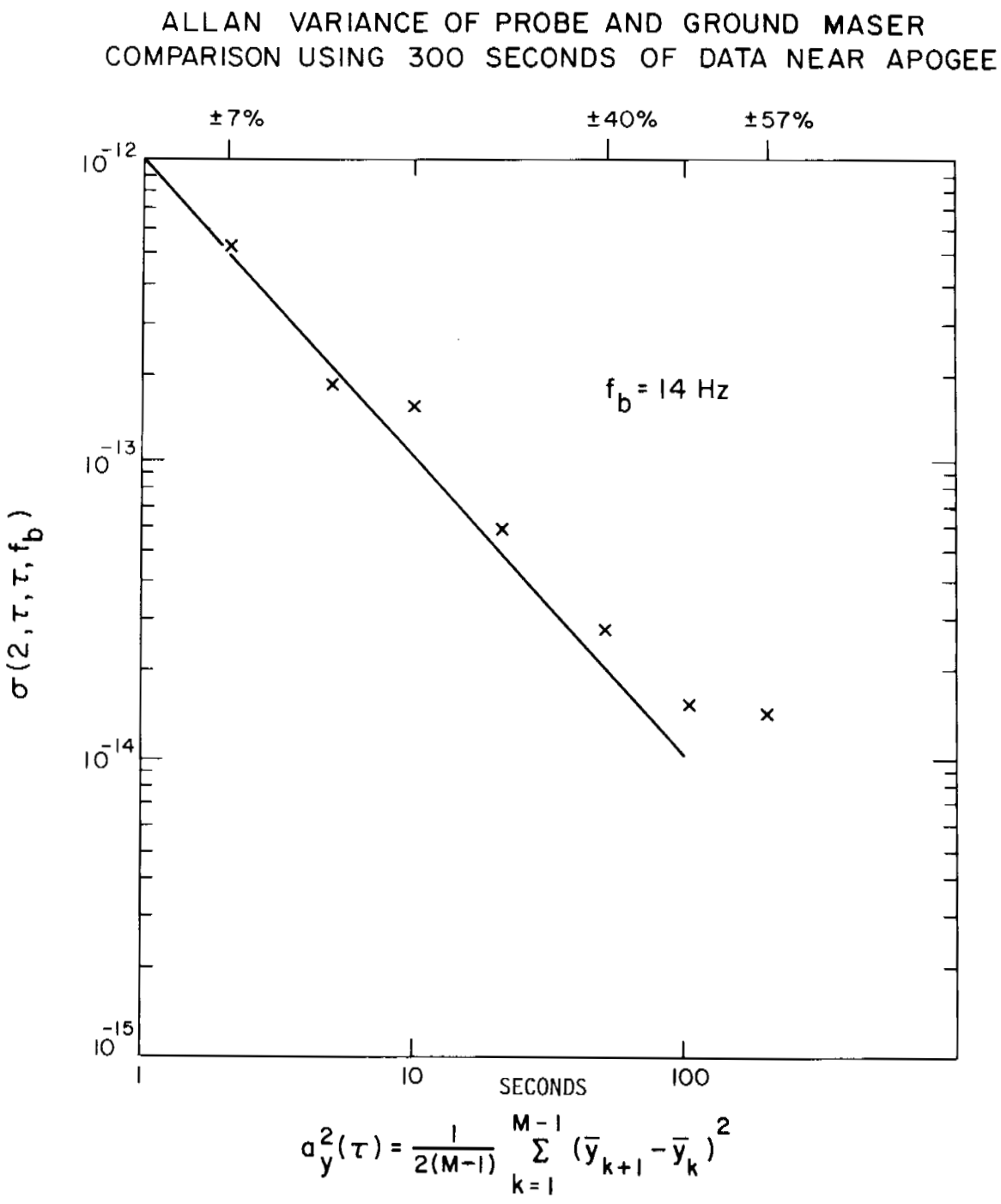

Fig. 21 Allan variance of the redshift beat frequency near apogee, taken from the system shown in Fig. 1.

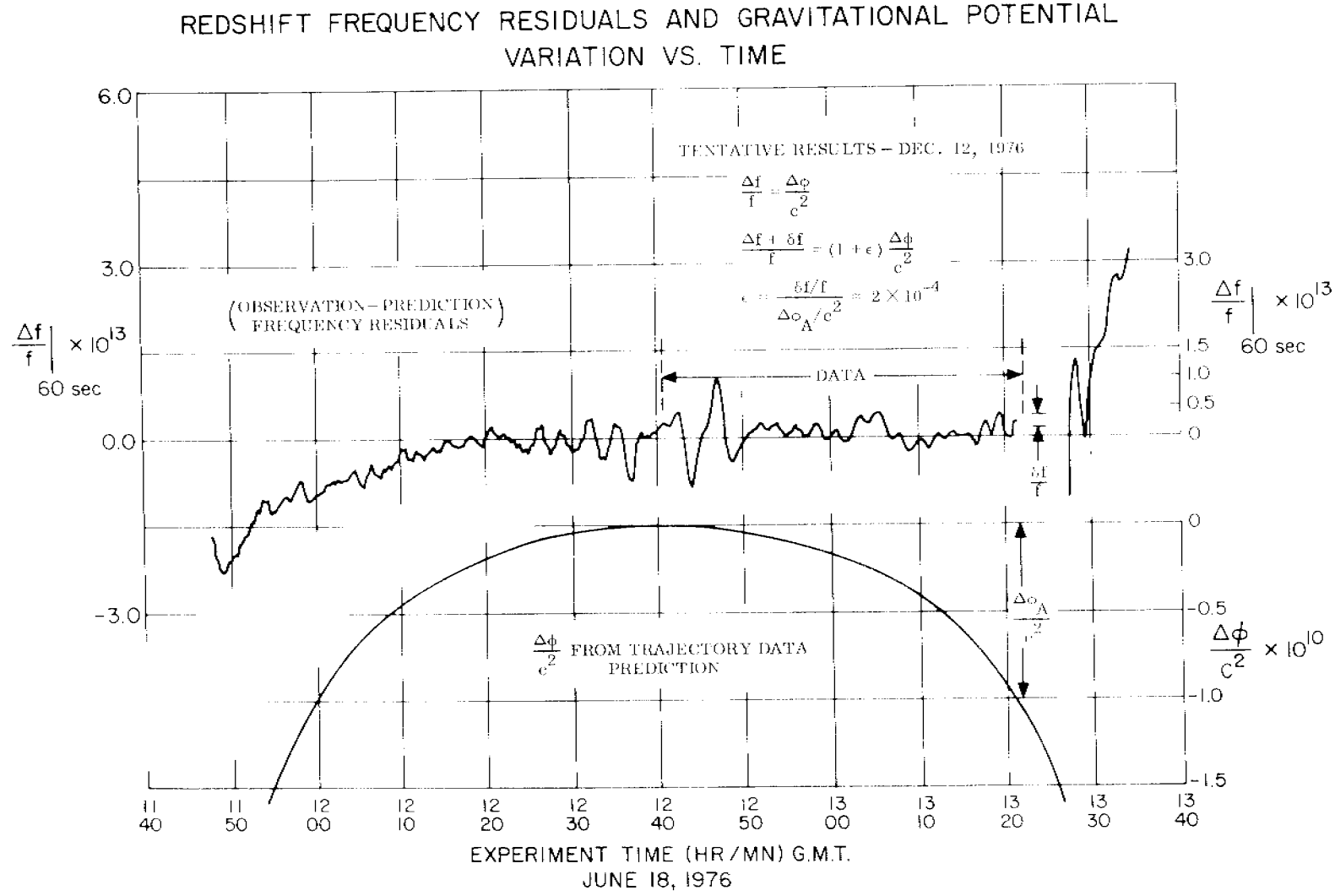

Fig. 22 Data from the preliminary payload trajectory.